FACULTY OF TECHNOLOGY

AMAR TELIDJI UNIVERSITY

Master degree

Title

DEEP SPACE ANTENNA POSITION CONTROL USING OPTIMIZED PID WITH ARTIFICIAL INTELLIGENCE

Defended on 20/06/2026

Presented by

MOHAMMED Boucif

Director

Pof. Mohammed Silaa

University season:2025/2026

بسم الله الرحمن الرحيم

In the Name of Allah

The Most Merciful The Most Compassionate

DEEP SPACE ANTENNA POSITION CONTROL USING OPTIMIZED PID WITH ARTIFICIAL INTELLIGENCE

By Islam Bousif

A thesis submitted for the requirement of the degree of .....
(Department/Minor Specialization)

Supervised By
Dr. Mohammed Yousri Silaa

FACULTY OF TECHNOLOGY
AMAR TELIDJI UNIVERSITY
ALGERIA
2025/2026

TITLE

By (Author)

This thesis has been approved and accepted in partial fulfillment of the requirements for the degree of .....
(Department/Minor Specialization)

EXAMINATION COMMITTEE

	Name	Rank	Field	Signature
Internal Examiner				
External Examiner				
Co-Advisor				
Advisor				

Dedication

To my beloved family, who have been my first source of support and strength throughout all stages of my life, and to everyone who believed in me and encouraged me to continue this academic journey.

To my respected professors, who generously shared their knowledge and guidance, and to all those who contributed, directly or indirectly, to the completion of this work.

I dedicate this humble effort with deep gratitude and appreciation.

Acknowledgment

I am also deeply grateful to all my professors who contributed to my academic formation and provided me with the knowledge and tools necessary to carry out this work.

Special thanks go to my colleagues and friends for their support, discussions, and encouragement during this journey.

Finally, I would like to thank my family for their unconditional love, patience, and motivation, which have been my greatest source of strength throughout my studies.First and foremost, I would like to express my sincere gratitude to my supervisor, Dr. Mohammed Yousri Silaa, for his continuous guidance, valuable advice, and constant support throughout this research work. His expertise and encouragement were essential in the completion of this thesis.

I am also deeply grateful to all my professors who contributed to my academic formation and provided me with the knowledge and tools necessary to carry out this work.

Special thanks go to my colleagues and friends for their support, discussions, and encouragement during this journey.

Finally, I would like to thank my family for their unconditional love, patience, and motivation, which have been my greatest source of strength throughout my studies.

Abstract

This thesis presents the design, optimization, and comparative analysis of advanced control strategies for a two-axis (azimuth–elevation) antenna tracking system. The main objective is to improve tracking accuracy, dynamic response, and robustness under realistic operating conditions. To achieve this, several control approaches are investigated, including classical Proportional–Integral–Derivative (PID) controllers, Sliding Mode Control (SMC), and a hybrid SMC-PID scheme. In order to enhance controller performance, metaheuristic optimization algorithms, namely Particle Swarm Optimization (PSO), Grey Wolf Optimization (GWO), and Ant Colony Optimization (ACO), are employed to tune the controller parameters. The performance evaluation is conducted using the Integral of Time-weighted Absolute Error (ITAE) as the primary objective function, ensuring both fast transient response and minimal steady-state error. The simulation results demonstrate that classical tuning methods such as Ziegler–Nichols provide limited performance due to oscillations and slower convergence. In contrast, optimization-based PID controllers significantly improve system behavior, with ACO-PID achieving the best performance among standalone PID approaches. Furthermore, the integration of SMC with PID in a hybrid structure leads to superior results, combining robustness against disturbances with smooth tracking performance. The proposed ACO-SMC-PID controller exhibits the best overall performance, characterized by reduced tracking error, fast convergence, improved stability, and efficient control effort. The findings confirm that hybrid nonlinear control strategies optimized using metaheuristic algorithms provide an effective and reliable solution for high-precision antenna tracking applications.

Key words: Antenna tracking, PID control, Sliding Mode Control, Hybrid control, Ant Colony Optimization, Grey Wolf Optimization, Particle Swarm Optimization, ITAE, Metaheuristic optimization, Nonlinear control.

الملخص

تقدم هذه الأطروحة تصميمًا وتحسينًا وتحليلًا مقارنًا لاستراتيجيات التحكم المتقدمة لنظام تتبع هوائي ثنائي المحور (السمت–الارتفاع). الهدف الرئيسي هو تحسين دقة التتبع، والاستجابة الديناميكية، والمتانة تحت ظروف تشغيل واقعية. ولتحقيق ذلك، تم دراسة عدة أساليب تحكم تشمل المتحكم التقليدي التناسبي–التكاملي–التفاضلي ،(PID) والتحكم بالوضع الانزلاقي ،(SMC) بالإضافة إلى مخطط تحكم هجين يجمع بين SMC و .PID من أجل تحسين أداء المتحكمات، تم استخدام خوارزميات التحسين الاستكشافية (Metaheuristic Optimization) وهي: تحسين سرب الجسيمات ،(PSO) وتحسين الذئاب الرمادية ،(GWO) وخوارزمية مستعمرة النمل ،(ACO) وذلك لضبط معاملات المتحكمات بشكل أمثل. تم إجراء تقييم الأداء باستخدام معيار التكامل المطلق للخطأ الموزون بالزمن (ITAE) كدالة هدف رئيسية، مما يضمن استجابة سريعة وتقليل الخطأ في الحالة المستقرة. تُظهر نتائج المحاكاة أن طرق الضبط التقليدية مثل Ziegler–Nichols تعطي أداءً محدودًا بسبب التذبذب وبطء الاستقرار. في المقابل، تحسن المتحكمات PID المعتمدة على التحسين بشكل كبير من أداء النظام، حيث حقق متحكم ACO-PID أفضل أداء بين المتحكمات PID المستقلة. علاوة على ذلك، فإن دمج التحكم بالوضع الانزلاقي مع PID في بنية هجينة يؤدي إلى نتائج أفضل، حيث يجمع بين المتانة ضد الاضطرابات وسلاسة التتبع. وقد أظهر المتحكم المقترح ACO-SMC-PID أفضل أداء شامل، يتمثل في تقليل خطأ التتبع، وسرعة التقارب، وتحسين الاستقرار، وكفاءة في جهد التحكم. تؤكد النتائج أن استراتيجيات التحكم غير الخطية الهجينة، المحسّنة باستخدام خوارزميات التحسين الاستكشافية، تمثل حلاً فعالًا وموثوقًا لتطبيقات تتبع الهوائيات عالية الدقة.

الكلمات المفتاحية: التحكم بالوضع الانزلاقي، تحكم هجين، تحسين مستعمرة النمل، تحسين الذئاب الرمادية، تحسين سرب الجسيمات، ITAE، التحسين الاستكشافي، التحكم غير الخطي

TABLE OF CONTENTS

Copyright 1

Dedication 1

Acknowledgment vii

Abstract viii

المستخلص ix

TABLE OF CONTENTS xii

LIST OF FIGURES xiii

LIST OF TABLES xiv

LIST OF SYMBOLS xv

Chapter 1 General introduction 1

1.1 Background 1
1.2 Literature review 3
1.3 Motivation 4
1.4 Problem statement 5
1.5 Research gap 5
1.6 Objectives 6
1.7 Contributions 7
1.8 Thesis Structure 8

Chapter 2 Deep space antenna modeling 9

2.1 Introduction 9
2.2 System Description 11
2.2.1 Antenna Structure 11
2.2.2 Actuation System 12
2.2.3 Block Diagram of the Antenna Tracking System 13
2.3 Modeling Assumptions 14
2.4 DC Motor Mathematical Model 15

2.5 State-Space Modeling (Single Axis First) . . . 16
2.6 Extension to 2-Axis System (AZ/EL) . . . 18
2.7 System Constraints . . . 21
2.7.1 Actuator Saturation . . . 21
2.7.2 Angular Velocity Limits . . . 21
2.7.3 Acceleration Limits . . . 21
2.7.4 Wind Disturbance . . . 22
2.7.5 Mechanical Backlash . . . 22
2.8 Conclusion . . . 22

Chapter 3 Control Techniques 24
3.1 Introduction . . . 24
3.2 Proportional-Integral (PI) Controller . . . 24
3.2.1 Control Law . . . 25
3.2.2 Closed-Loop PI Control Structure . . . 25
3.2.3 Transfer Function Representation . . . 25
3.2.4 Role of Each Term . . . 26
3.2.5 Advantages . . . 26
3.2.6 Limitations . . . 26
3.2.7 Remarks . . . 26
3.3 Proportional-Derivative (PD) Controller . . . 26
3.3.1 Control Law . . . 26
3.3.2 Closed-Loop PD Control Structure . . . 27
3.3.3 Transfer Function Representation . . . 27
3.3.4 Role of Each Term . . . 27
3.3.5 Advantages . . . 27
3.3.6 Limitations . . . 28
3.3.7 Remarks . . . 28
3.4 Proportional-Integral-Derivative (PID) Controller . . . 28
3.4.1 Control Law . . . 28
3.4.2 Closed-Loop PID Control Structure . . . 28
3.4.3 Transfer Function Representation . . . 29
3.4.4 Role of Each Term . . . 29
3.4.5 Advantages . . . 29
3.4.6 Limitations . . . 30
3.4.7 Remarks . . . 30
3.5 Sliding Mode Control (SMC) . . . 30
3.5.1 System Description . . . 31
3.5.2 Sliding Surface Design . . . 31
3.5.3 SMC Control Law . . . 32
3.5.3.1 Equivalent Control . . . 32
3.5.3.2 Switching Control . . . 32
3.5.4 Reaching Condition . . . 32
3.5.5 Advantages and Limitations . . . 33

3.6 Conclusion . . . 33

Chapter 4 Tuning and Optimization Techniques 34
4.1 Introduction . . . 34
4.1.1 Ziegler–Nichols Tuning Method . . . 35
4.1.1.1 Ultimate Gain Method . . . 35
4.1.1.2 Step Response Method . . . 36
4.1.1.3 Advantages and Limitations of the ZN Method . . . 36
4.2 Metaheuristic Optimization Techniques . . . 37
4.2.1 Particle Swarm Optimization (PSO) . . . 37
4.2.2 Grey Wolf Optimization (GWO) . . . 39
4.2.2.1 Social Hierarchy . . . 40
4.2.2.2 Encircling Behavior . . . 40
4.2.2.3 Hunting Mechanism . . . 40
4.2.2.4 Attacking the Prey . . . 41
4.2.3 Ant Colony Optimization (ACO) . . . 42
4.2.3.1 Solution Construction . . . 42
4.2.3.2 Pheromone Update . . . 43
4.2.3.3 Exploration and Exploitation . . . 43
4.2.3.4 Algorithm Procedure . . . 44
4.3 Conclusion . . . 45

Chapter 5 Results and Discussion 47
5.1 Introduction . . . 47
5.2 Results Analysis . . . 47
5.3 Conclusion . . . 53

Chapter 6 General Conclusions 54

References 56

List of Figures

1.1 Deep space ground antenna used for long-distance communication with spacecraft 1

2.1 Schematic of a deep space antenna showing azimuth and elevation axes and line-of-sight vector 10
2.2 Mechanical structure of the deep space antenna showing azimuth-elevation gimbal system and parabolic reflector 12
2.3 Electrical circuit and mechanical coupling of a DC motor 12
2.4 Block diagram of the deep space antenna tracking control system 14

3.1 Closed-loop structure of a PI control system 25
3.2 Closed-loop structure of a PD control system 27
3.3 Closed-loop structure of a PID control system 29
3.4 SMC sliding surface 30

4.1 Closed-loop ultimate gain tuning procedure 35
4.2 Open-loop step response tuning procedure 36
4.3 PSO particle movement in the search space 38
4.4 Flowchart of the PSO algorithm 39
4.5 Position updating mechanism of grey wolves and the effect of coefficient $\overrightarrow{A}$ 41
4.6 Flowchart of the GWO algorithm 42
4.7 Illustration of ant movement and pheromone trail formation 44
4.8 Flowchart of the Ant Colony Optimization algorithm 45

5.1 Control signals under different approaches 49
5.2 Error signals under different approaches 50
5.3 Velocities signals under different approaches 51
5.4 Positions signals under different approaches 52

List of Tables

4.1 Ziegler–Nichols tuning rules based on the ultimate gain method. 35
4.2 Ziegler–Nichols tuning rules based on the step response method. 36

5.1 PSO-PID and GWO-PID Gains 48
5.2 ACO-PID Optimal Gains 48
5.3 ACO-SMC-PID Gains 48
5.4 Ziegler–Nichols PID Gains 48
5.5 ITAE Performance Comparison 53

LIST OF ABBREVIATIONS

ACO	Ant Colony Optimization
GWO	Grey Wolf Optimization
PSO	Particle Swarm Optimization
PID	Proportional–Integral–Derivative
SMC	Sliding Mode Control
SMCPID	Sliding Mode Control with PID
ZN	Ziegler–Nichols
ITAE	Integral of Time-weighted Absolute Error
LOS	Line of Sight
AZ	Azimuth Axis
EL	Elevation Axis
DOF	Degrees of Freedom
ODE	Ordinary Differential Equation
RMSE	Root Mean Square Error
IAE	Integral of Absolute Error
ISE	Integral of Squared Error
K_p	Proportional Gain
K_i	Integral Gain
K_d	Derivative Gain
λ	Sliding Surface Slope
K_{smc}	Sliding Mode Gain

Chapter 1

General introduction

1.1 Background

Deep space communication plays a critical role in modern space exploration, enabling the transfer of scientific data, telemetry, and commands between spacecraft operating far from Earth and mission control centers. Spacecraft exploring the Moon, Mars, asteroids, or outer planets rely on reliable communication links to ensure mission success [1]. The distances involved in deep space missions are immense, often spanning millions or even billions of kilometers, which causes transmitted signals to weaken dramatically due to free-space path loss. Therefore, highly sensitive ground-based antennas and advanced communication technologies are essential to maintain contact with spacecraft and retrieve valuable scientific data [2].



Figure 1.1: Deep space ground antenna used for long-distance communication with spacecraft

Deep space communication enables several critical functions for interplanetary missions. First, it allows mission controllers to monitor spacecraft health and operational status by receiving telemetry data that includes power levels, thermal conditions, and instrument

readings. This information is crucial for diagnosing issues and performing corrective actions during long-duration missions [2]. Second, deep space communication provides the primary means of navigation and trajectory control, as precise Doppler and range measurements are used to track spacecraft position and velocity, allowing accurate course corrections for planetary flybys, orbital insertions, and rendezvous operations (NASA DSN, 2023) [3]. Finally, communication links facilitate the return of scientific data, including high-resolution images, atmospheric measurements, and instrument readings, which expand our knowledge of planetary systems and the universe beyond Earth. Maintaining precise alignment between ground-based antennas and distant spacecraft is one of the most significant challenges in deep space communication. High-gain antennas are characterized by extremely narrow beamwidths, which makes them highly sensitive to even small angular errors [3]. Mechanical disturbances, such as friction, backlash, and wind, as well as dynamic changes in the spacecraft trajectory, can introduce pointing errors that reduce signal strength and degrade communication quality. Furthermore, the long distances involved result in signal propagation delays, which necessitate predictive or feedforward tracking techniques to ensure the antenna remains accurately aligned with the moving spacecraft. The Deep Space Network (DSN) antennas themselves have evolved over decades to meet increasing mission demands [3]:

- 1958: The first DSN antenna, a 26-m L-band dish, began operation to support Pioneers 3 and 4. Initially equipped with a focal-point feed system, it was soon converted to a Cassegrain configuration.
- 1962: The Echo antenna, originally 26 m in diameter, was erected at the Goldstone site and later extended to 34 m in 1979. The Venus site also began operations as the DSN research and development station.
- 1966: The first 64-m antenna was completed, scaled up from the 26-m design, and initially operated at S-band (2.11–2.12 GHz transmit and 2.27–2.30 GHz receive).
- 1968: An X-band feed cone was installed to enable improved multifrequency operation. Feed structures were modified to allow rapid switching between different feed cones using an asymmetrically truncated subreflector.
- 1982: Introduction of the 34-m High-Efficiency (HEF) antenna with a common-aperture feed horn and dual-shaped optics, optimizing gain-to-noise ratio (G/T).
- 1985: The original Pioneer antenna site was declared a U.S. National Historic Landmark.
- 1989: For NASA's Voyager Neptune encounter, a 70-m antenna with dual-shaped optics and high-precision panels was deployed to enhance performance.
- 1990s: Research demonstrated Ka-band operation on the 70-m antennas, improving data rates and enabling advanced scientific measurements.

- 2000: X-band uplink capability (7.145–7.190 GHz) was added to the 70-m antennas to support modern deep space missions.

These milestones highlight the continuous evolution of DSN antennas, driven by the increasing need for high-gain, narrow-beam communication systems capable of supporting increasingly complex and distant spacecraft missions. Each technological innovation — from larger dish sizes to advanced feed systems was aimed at improving pointing accuracy, gain, and overall system performance. High-gain antennas are essential for deep space missions because they amplify the weak signals transmitted over vast distances. However, their narrow beamwidth imposes stringent constraints on pointing accuracy. The half-power beamwidth of a parabolic antenna is inversely proportional to its diameter and operating frequency, meaning that larger antennas or higher frequencies result in narrower beams [4]. This requirement for extreme precision challenges both mechanical design and control systems, as any deviation from the desired pointing direction leads to significant pointing loss, reducing the effective gain of the antenna. Consequently, advanced control strategies are required to ensure that the antenna maintains high pointing accuracy, compensates for disturbances, and reliably tracks the spacecraft. Deep-space communication is indispensable for mission success, yet it presents significant challenges due to the extreme distances, weak signals, and the precision required in antenna pointing and tracking. These challenges motivate the need for robust, optimized control strategies capable of maintaining accurate alignment and maximizing communication performance [5].

1.2 Literature review

In the field of control engineering, classical linear controllers such as Proportional Integral (PI), Proportional Derivative (PD), and Proportional Integral Derivative (PID) controllers have long been fundamental due to their relative simplicity and effectiveness in many single-input single-output (SISO) systems [6]. PI controllers effectively eliminate steady-state errors by integrating the accumulated error over time, making them particularly suitable for systems where offset must be minimized, while PD controllers improve transient response, providing faster damping and reduced overshoot in systems where error rate dynamics matter. The combination of these actions in a PID controller leverages the advantages of proportional, integral, and derivative terms, achieving a balanced performance in terms of accuracy, speed, and stability. However, all these controllers require careful tuning of their respective gains to balance stability, responsiveness, and robustness, and heuristic tuning methods such as the Ziegler–Nichols rules are often employed as starting points in practice [7,8]. Because PI, PD, and PID controllers lack explicit model knowledge of the processes they govern, optimization methods have been widely explored to systematically determine optimal gain parameters that minimize performance indices such as rise time, overshoot, and steady-state error. In addition to Particle Swarm Optimization (PSO), various metaheuristic techniques such as Genetic Algorithms (GA), Grey Wolf Optimizer (GWO), Ant Colony Optimization (ACO), and Differential Evolution (DE) have been successfully applied to tune controller parameters. These approaches enable automated and efficient search of the parameter space, resulting in improved dynamic

responses and enhanced robustness compared to manually tuned gains [9–13]. Moreover, hybrid structures that combine PD with optimal control frameworks, such as tuning PD gains within a Linear Quadratic Regulator (LQR) architecture using metaheuristic methods like Biogeography Based Optimization (BBO), have demonstrated that combining classical control with optimal criteria can yield superior performance in transient behavior and robustness relative to standalone PD or LQR designs [14]. LQR itself represents a staple of optimal control theory, formulating control design as the minimization of a quadratic cost function over state and control effort and providing inherent robustness and guaranteed gain and phase margins for linear systems; its effectiveness makes it a popular choice for multi input multi output (MIMO) systems, though the selection of its weighting matrices (Q and R) often necessitates additional tuning or optimization to balance performance trade offs [15]. Beyond linear approaches, Sliding Mode Control (SMC) is recognized as a robust nonlinear control strategy that forces system trajectories onto a predefined sliding surface, offering strong disturbance rejection and insensitivity to parameter variations, which is particularly valuable in uncertain or highly nonlinear environments [16]. The main drawback of classical SMC is the so-called chattering phenomenon, characterized by high-frequency oscillations around the sliding surface. To mitigate this issue, many researchers have proposed advanced approaches, including high-order sliding mode control (HOSMC), which shifts the discontinuity to higher derivatives of the control signal, significantly reducing chattering while preserving robustness. In addition, adaptive laws and hybrid strategies integrating fuzzy logic, adaptive or neural networks have also been employed to achieve smoother control actions and improved performance [17–19]. Comparative studies across these controller types (PI, PD, LQR, SMC, HOSMC) in various applications, such as DC converters, servo motors, or robotic manipulators, illustrate that while simple proportional based controllers can suffice for systems with mild nonlinearity or well known dynamics, optimal and robust controllers like LQR and SMC generally achieve better performance under disturbances and model uncertainties; however, they may require more sophisticated tuning, modeling efforts, or optimization routines. In the context of advanced control for precision systems (e.g., deep space antenna tracking), optimization-assisted tuning and hybrid controllers that blend the strengths of classical and robust or optimal techniques continue to attract significant research attention, as they offer pathways to enhanced precision, stability, and robustness that individual classical controllers struggle to deliver alone [20].

1.3 Motivation

The success of deep space missions critically depends on the ability to maintain reliable communication links between spacecraft and ground stations. Due to the immense distances involved, the signals transmitted by spacecraft are extremely weak when they reach Earth. High-gain antennas with narrow beamwidths are required to capture these signals effectively; however, their narrow beams make the system highly sensitive to misalignment or pointing errors. Even small deviations in antenna orientation can cause a significant reduction in received signal strength, leading to loss of data, degraded telemetry, and compromised

scientific measurements. Therefore, precise positioning and accurate tracking of the antenna are essential to ensure mission success and maximize the quality of the communication link.

Traditional control strategies, such as manually tuned PID controllers or classical systems, have been widely employed for antenna positioning. While these methods are simple and computationally efficient, they often struggle to maintain optimal performance under real-world conditions. Mechanical disturbances such as friction, backlash, wind gusts, and thermal expansion introduce non-linearities and uncertainties that conventional controllers may not handle effectively. Furthermore, fixed PID gains that are tuned for nominal conditions may fail to provide adequate tracking performance under varying operational scenarios, resulting in slow response, overshoot, or residual steady-state error.

The increasing complexity of deep space missions, combined with the stringent requirements for high-gain, narrow-beam antennas, highlights the need for advanced control strategies capable of optimizing performance automatically. Intelligent and metaheuristic optimization methods, such as Ant Colony Optimization (ACO), offer a promising approach for tuning controller parameters, enhancing robustness, and improving pointing accuracy. By integrating classical control techniques with optimization algorithms, it becomes possible to overcome the limitations of conventional methods and ensure reliable, high-quality communication links over vast interplanetary distances.

1.4 Problem statement

Maintaining precise orientation of a deep space antenna is challenging due to:

- Mechanical disturbances (backlash, friction, wind)
- Nonlinear dynamics of azimuth-elevation drives
- Wide range of operating conditions
- Classical PID tuning is inadequate for all scenarios.

Objective: Develop a control strategy that ensures optimal antenna pointing using PID with optimization tuning techniques.

1.5 Research gap

Despite extensive research on deep space antenna control using classical techniques such as PID, sliding mode, and robust controllers, several critical limitations remain. Most existing studies focus on tuning controller parameters using a single optimization algorithm, often targeting only one performance metric such as tracking error, while neglecting others like control energy consumption, robustness to disturbances, and system response time. Furthermore, hybrid optimization approaches that combine multiple algorithms to enhance performance have been scarcely explored. Additionally, many works are limited to simulation studies with simplified models of antenna dynamics, and realistic environmental disturbances such as structural vibrations, thermal effects, and wind are often underrepresented.

These limitations indicate a clear need for a comprehensive investigation that compares different optimization techniques, explores hybrid and multi-objective optimization strategies, and evaluates performance under more realistic operational conditions. Addressing these gaps will contribute to the development of more efficient, robust, and reliable deep space antenna control systems.

1.6 Objectives

The primary objective of this thesis is to develop an efficient and robust position control system for a deep space antenna that ensures high pointing accuracy and reliable communication with distant spacecraft. To achieve this, the study focuses on the following specific objectives:

1. **Model the dynamics of a deep space antenna**
    - Develop a mathematical and mechanical model representing the azimuth and elevation movements of the antenna.
    - Include key dynamic factors such as inertia, damping, and external disturbances that influence antenna motion.
2. **Design a PID controller for azimuth and elevation control**
    - Implement classical PID controllers to regulate the antenna's position along both axes.
    - Establish control laws that minimize pointing error while ensuring system stability.
3. **Optimize PID parameters using optimization techniques**
    - Apply the Ant Colony Optimization (ACO) metaheuristic algorithm to automatically tune the PID gains for optimal performance.
    - Define a suitable fitness function that considers pointing error, response time, and robustness.
4. **Evaluate the performance of the proposed control system**

    The system will be assessed under various operating conditions using the following performance metrics:

    - **Pointing accuracy:** Ensure the antenna maintains precise alignment with the target spacecraft, minimizing angular errors.
    - **Response time:** Achieve fast settling to the desired position with minimal overshoot.
    - **Disturbance rejection:** Maintain stability and tracking performance under external disturbances such as wind or mechanical friction.

- **Robustness:** Verify consistent performance under variations in system parameters or operating conditions.

By systematically addressing these objectives, this thesis aims to demonstrate the effectiveness of optimized PID control in enhancing the precision and reliability of deep space antenna positioning systems, thereby improving communication link quality with distant spacecraft.

1.7 Contributions

This thesis makes several key contributions to the field of deep space antenna control by integrating classical control techniques with metaheuristic optimization. The main contributions are summarized as follows:

1. **Development of a PID-based position control system for a deep space antenna**
    - A robust control framework has been designed to regulate the azimuth and elevation movements of the antenna.
    - The PID controller ensures accurate tracking of the spacecraft's line-of-sight while maintaining system stability.
2. **Implementation of optimization techniques for PID parameter optimization**
    - The thesis applies the Ant Colony Optimization (ACO) algorithm to automatically tune the PID gains, overcoming the limitations of manual tuning.
    - The optimization process considers key performance metrics, such as pointing accuracy, response time, and disturbance rejection, to achieve optimal control performance.
3. **Demonstration of improved performance compared to manually tuned PID controllers**
    - Through simulation studies, the proposed optimized PID system exhibits enhanced tracking accuracy and faster response compared to conventional PID controllers.
    - The results highlight the advantages of integrating metaheuristic optimization with classical control methods for high-precision applications.
4. **Simulation and analysis of system performance under various operating conditions**
    - The study provides a detailed analysis of tracking error, overshoot, and settling time under different disturbances and parameter variations.
    - This evaluation demonstrates the robustness and reliability of the proposed control strategy, ensuring its applicability for real-world deep space communication scenarios.

In summary, the thesis presents a comprehensive methodology for improving deep space antenna positioning, combining PID control with optimization techniques to enhance pointing precision, dynamic response, and robustness, ultimately contributing to more reliable and effective deep space communication.

1.8 Thesis Structure

The remainder of this thesis is organized into six chapters, each addressing a critical aspect of the design, implementation, and evaluation of a deep space antenna position control system. Chapter 2 presents a detailed mathematical and mechanical model of the deep space antenna, covering the dynamics of the azimuth and elevation axes, the formulation of the line-of-sight vector, and the analysis of pointing errors, thereby establishing the foundation for control system design. Chapter 3 focuses on control techniques and design, where classical and modern strategies for antenna positioning are developed; in particular, the PID controller for azimuth and elevation control is introduced, its limitations are discussed, and the groundwork for performance enhancement through optimization is established. Chapter 4 is devoted to optimization techniques, highlighting metaheuristic approaches for tuning PID, SMC, and the optimized PID parameters. Chapter 5 presents simulation results and performance evaluation of the proposed control system, including a comparative analysis between classical PID, SMC, and optimized PID controllers based on key metrics such as pointing accuracy, response time, disturbance rejection, and robustness under various operating conditions. Finally, Chapter 6 presents the general conclusions of this thesis, summarizing the main findings and key contributions. It also highlights potential directions for future research, including multi-objective optimization and the integration of advanced control strategies.

Chapter 2

Deep space antenna modeling

2.1 Introduction

Modeling the electromechanical dynamics of a deep space antenna is a fundamental step in the design and analysis of high-precision tracking systems. Deep space antennas are large ground-based parabolic structures used to communicate with spacecraft operating millions or even billions of kilometers from Earth. Unlike conventional antennas, deep space antennas require extremely high gain and very narrow beamwidths, making them highly sensitive to even small angular deviations in pointing direction. Therefore, accurate system modeling is essential to understand how the antenna responds to control inputs, disturbances, and parameter uncertainties, ensuring reliable communication over vast distances [21].

This chapter focuses on the dynamic modeling of the deep space antenna tracking system, highlighting its electromechanical nature. The antenna is typically mounted on an azimuth-elevation (AZ-EL) gimbal structure, which enables rotation around two orthogonal axes: the azimuth axis (horizontal motion) and the elevation axis (vertical motion). Each axis is driven by an actuator, typically a DC motor coupled through a gear transmission system. The system behavior is therefore governed by the interaction between electrical dynamics (armature circuit), mechanical dynamics (rotational motion), and electromechanical coupling effects. For each axis, the DC motor converts electrical energy into mechanical torque through the armature current, while the rotational motion generates a back electromotive force (back-EMF) that influences the electrical subsystem. This coupling results in a nonlinear but commonly linearized electromechanical model, where the antenna angle, angular velocity, and motor current are considered as the main state variables.

The dynamics of each axis are influenced by physical parameters such as inertia, viscous friction, motor torque constant, and electrical resistance and inductance. Additionally, external disturbances such as wind loading, structural vibrations, and mechanical friction can affect system performance. Incorporating these effects provides a realistic representation of antenna behavior under operational conditions. The model also considers practical operational constraints, including maximum angular velocity, acceleration limits, actuator saturation, and mechanical nonlinearities such as backlash, stiction, and structural flexibility. These constraints are critical for ensuring stable operation, avoiding overshoot, and maintain-

ing precise pointing accuracy during long-duration deep space missions [4].

Furthermore, the developed model establishes the relationship between antenna motion and the line-of-sight (LOS) vector directed toward the spacecraft. This relationship is essential for computing pointing errors, which form the basis of feedback control in tracking systems. The resulting mathematical representation is typically expressed in state-space form, which is suitable for modern control design techniques such as PID, LQR, and Kalman filtering. Figure 2.1 illustrates the mechanical structure of a typical deep space antenna, showing the azimuth and elevation axes, the gimbal system, and the line-of-sight vector pointing towards a spacecraft.

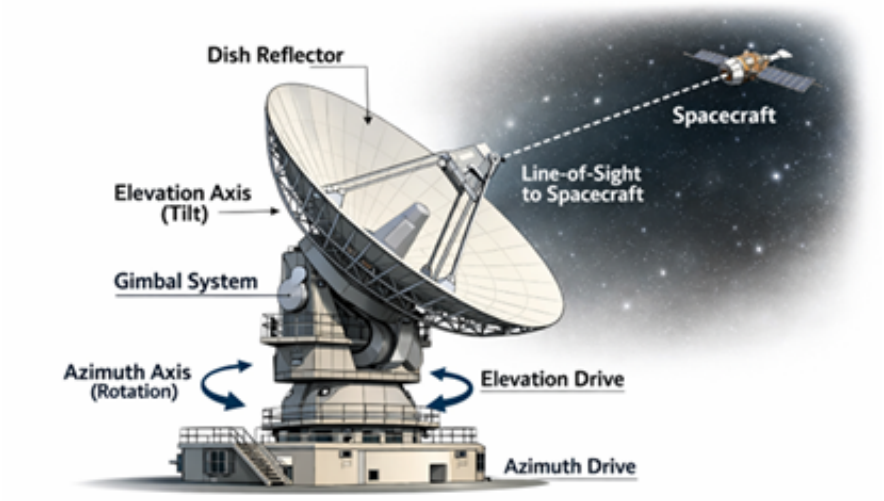


Figure 2.1: Schematic of a deep space antenna showing azimuth and elevation axes and line-of-sight vector

In position control systems for antenna applications, different types of actuators can be used, such as DC motors, stepper motors, or servo systems. The selection of the appropriate actuator depends on the required torque, speed response, and positioning accuracy. In this work, a DC motor is adopted as the main actuator due to its simplicity, reliability, and well-established control modeling framework. The operating principle of the DC motor is based on electromechanical energy conversion, where the applied armature voltage generates a current that produces electromagnetic torque. This torque drives the mechanical rotation of the antenna, while the back-EMF provides an internal feedback mechanism linking mechanical motion to electrical behavior. In summary, this section presents the electromechanical modeling framework of the deep space antenna tracking system. The developed model captures both the electrical and mechanical dynamics of the DC motor-driven AZ-EL structure, as well as the operational constraints and disturbances affecting system performance. This modeling foundation is essential for the subsequent development of precise tracking control strategies required to maintain reliable communication with distant spacecraft [22].

2.2 System Description

The deep space antenna tracking system is a highly precise electromechanical system designed to maintain continuous alignment between a ground-based parabolic antenna and a distant spacecraft. Due to the extremely narrow beamwidth associated with high-frequency deep space communication links, even small angular deviations can result in significant signal degradation or complete link loss. For this reason, the system relies on a closed-loop tracking architecture that combines trajectory reference generation, real-time error estimation, and high-performance servo control. The following subsections describe the main physical and control components of the system, starting with the antenna mechanical structure [23].

2.2.1 Antenna Structure

The deep space antenna considered in this work is a large parabolic reflector system designed for high-gain, narrow-beamwidth communication with distant spacecraft. Its mechanical structure is composed of a rigid parabolic dish mounted on a two-axis azimuth-elevation (AZ-EL) gimbal system, which enables precise orientation of the antenna in space. The azimuth axis allows horizontal rotation of the antenna around the vertical axis, covering a full 360° range of motion. This motion is typically implemented using a high-torque DC motor coupled with a gear reduction system to ensure sufficient positioning accuracy and load handling capability. The elevation axis controls the vertical tilt of the antenna, enabling it to point from the horizon (0°) to the zenith (90°). Similar to the azimuth axis, the elevation motion is driven by a DC motor and gear assembly designed to support the antenna's large moment of inertia. The parabolic reflector is the main radiating and receiving element of the system. It is designed to focus electromagnetic waves onto the feed antenna located at the focal point of the parabola. Due to the high operating frequencies used in deep space communication (typically S-band, X-band, or Ka-band), the antenna exhibits a very narrow beamwidth, making precise mechanical pointing essential for maintaining a stable communication link. The entire structure is mounted on a rigid base to minimize vibrations and mechanical deflections caused by environmental disturbances such as wind loads or ground motion. However, small structural deformations and mechanical flexibilities still exist and may influence the pointing accuracy, especially in large antennas. Each axis is equipped with high-resolution encoders that measure the angular position of the antenna in real time. These measurements are used as feedback signals in the control system to ensure accurate tracking of the desired line-of-sight direction toward the spacecraft. Figure 2.2 illustrates the general configuration of the antenna system, showing the parabolic reflector, azimuth and elevation axes, and the mechanical gimbal structure [23, 24].

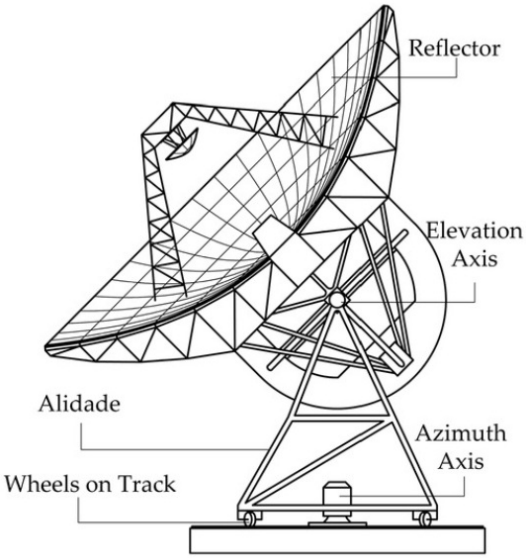


Figure 2.2: Mechanical structure of the deep space antenna showing azimuth-elevation gimbal system and parabolic reflector

The antenna structure is a two-degree-of-freedom (2-DOF) mechanical system designed to provide precise orientation of a high-gain parabolic reflector. Its mechanical configuration forms the basis for the electromechanical modeling and control design presented in the following sections.

2.2.2 Actuation System

The actuation system of the deep space antenna is modeled using the electromechanical DC motor configuration shown in Figure 2.3. The system consists of an electrical armature circuit coupled to a mechanical rotational load representing the antenna axis. The electrical and mechanical coupling of the DC motor is illustrated in Figure 2.3 [25].

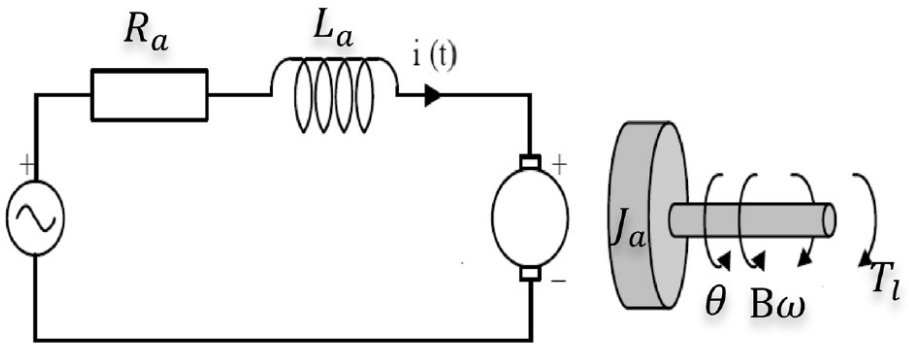


Figure 2.3: Electrical circuit and mechanical coupling of a DC motor

As illustrated in Figure 2.3, the electrical subsystem is composed of an applied voltage source $V_a(t)$, an armature resistance R_a, and an armature inductance L_a. The resulting armature current $i(t)$ generates the electromagnetic torque required to drive the antenna motion. The electrical dynamics of the system are given by [25]:

$$V_a(t) = R_a i(t) + L_a \frac{di(t)}{dt} + K_e \omega(t) \tag{2.1}$$

Where, $K_e\omega(t)$ represents the back electromotive force induced by the rotational motion of the motor. The mechanical part of the system, shown on the right side of Figure 2.3, consists of the equivalent inertia J_a, viscous friction $B\omega(t)$, the output angular position $\theta(t)$, and an external load torque $\tau_l(t)$ representing disturbances such as wind effects and structural resistance. The mechanical dynamics are described by [25]:

$$J_a \frac{d\omega(t)}{dt} + B\omega(t) = \tau(t) - \tau_l(t) \tag{2.2}$$

Where the electromagnetic torque is given by [25]:

$$\tau(t) = K_t i(t) \tag{2.3}$$

The angular position of the antenna axis is obtained from

$$\dot{\theta}(t) = \omega(t) \tag{2.4}$$

The diagram clearly illustrates the coupling between the electrical and mechanical domains. The armature current $i(t)$ generates torque $\tau(t)$, which drives the rotational motion of the antenna characterized by $\theta(t)$. Conversely, the rotational motion generates a back-EMF proportional to $\omega(t)$, which influences the electrical subsystem. This electromechanical interaction forms the basis of the antenna actuation system and is essential for deriving the state-space representation used in control system design.

2.2.3 Block Diagram of the Antenna Tracking System

The deep space antenna tracking system can be represented using a closed-loop control architecture, where the objective is to ensure that the antenna pointing angles (azimuth and elevation) accurately follow a time-varying reference generated from spacecraft ephemeris data. The overall system integrates a reference generator, a control law, an electromechanical actuator (DC motor), and a feedback measurement system [26]. Figure 2.4 illustrates the general block diagram of the antenna position control system.

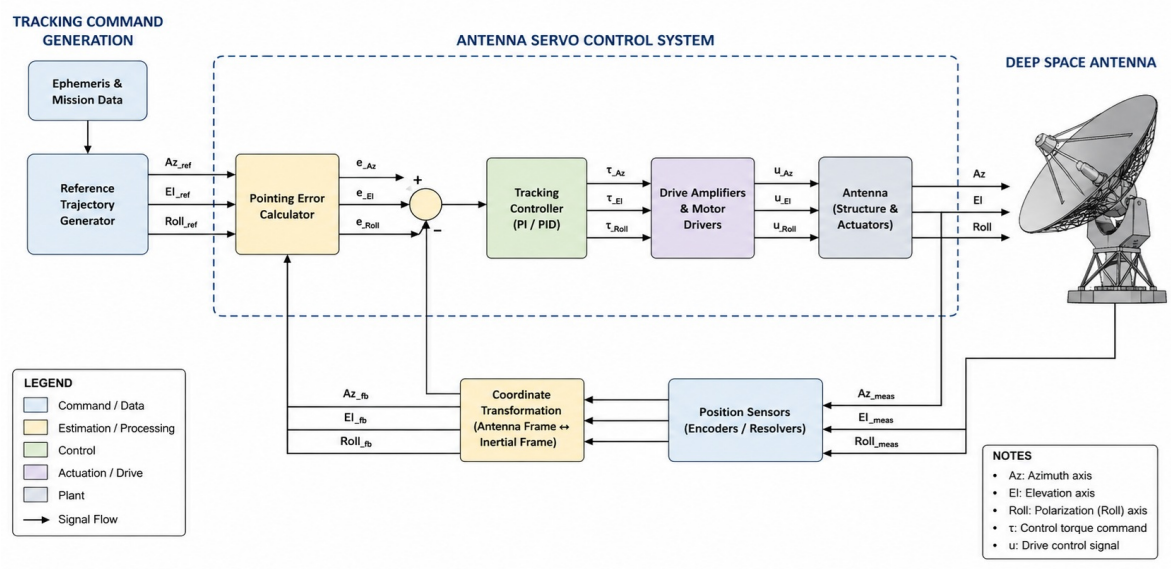


Figure 2.4: Block diagram of the deep space antenna tracking control system

The system operates as a closed-loop feedback structure. The reference input represents the desired antenna pointing angles, denoted as $\theta_{ref}(t)$, which are computed from the predicted position of the spacecraft. These reference angles are continuously compared with the actual antenna position $\theta(t)$, measured using high-resolution encoders mounted on each axis. The resulting tracking error is defined as follows:

$$e(t) = \theta_{ref}(t) - \theta(t) \tag{2.5}$$

This error signal is processed by the controller, which generates the appropriate control input voltage $V_a(t)$ for the DC motor. The controller may be implemented using classical or modern techniques such as PID, state feedback, or optimal control (LQR), depending on the required performance specifications. The DC motor acts as the actuator of the system, converting the electrical input $V_a(t)$ into mechanical torque $\tau(t)$. This torque drives the antenna through a mechanical transmission system, resulting in the angular displacement $\theta(t)$. The mechanical subsystem is affected by inertia J_a, viscous friction $B\omega(t)$, and external load disturbances $\tau_l(t)$, which may include wind effects and structural perturbations. The feedback loop is closed through angular position sensors that continuously measure $\theta(t)$ and provide real-time information to the controller. This closed-loop configuration ensures robustness against disturbances and model uncertainties, while maintaining the high pointing accuracy required for deep space communication. The block diagram highlights the interaction between the reference generation, control algorithm, electromechanical actuator, and feedback sensing system. This representation serves as the foundation for the mathematical modeling and control design developed in the subsequent sections [27].

2.3 Modeling Assumptions

In order to establish a tractable and physically consistent mathematical model of the deep space antenna system, several simplifying assumptions are introduced. These assump-

tions allow the system dynamics to be represented in a linear and analyzable form while preserving the essential behavior relevant to control design.

- First, the actuator is modeled as a linear DC motor, where the electrical and mechanical dynamics are assumed to follow standard linear relationships between voltage, current, torque, and angular velocity. This enables the use of well-known parameters such as armature resistance, inductance, and torque constant in the modeling process.
- Second, the antenna mechanical structure is considered rigid, meaning that structural flexibilities, vibrations, and deformations of the reflector and supporting arms are neglected. This assumption is reasonable for control-oriented modeling when the dominant dynamics are rotational rather than structural.
- Third, mechanical nonlinearities such as backlash in gears or transmission elements are neglected. This implies an ideal power transmission between the motor and antenna axis, without dead zones or hysteresis effects, simplifying the torque-to-motion relationship.
- Fourth, when angular displacements are small around the operating point, the small-angle approximation is applied. This allows linearization of trigonometric terms, which is particularly useful for simplifying the nonlinear rotational dynamics into linear differential equations.
- Finally, the azimuth (AZ) and elevation (EL) axes are assumed to be decoupled. In other words, the motion of one axis does not influence the dynamics of the other. This assumption enables independent single-input single-output (SISO) modeling of each axis, significantly reducing model complexity while maintaining sufficient accuracy for control design purposes.

2.4 DC Motor Mathematical Model

The DC motor used in the antenna actuation system is modeled as a coupled electromechanical system. The model is derived by combining the electrical dynamics of the armature circuit with the mechanical rotational dynamics of the motor shaft. This representation is essential for developing a control-oriented model of the antenna system. The electrical behavior of the armature circuit is governed by Kirchhoff's voltage law, which gives [25]:

$$V_a(t) = R_a i(t) + L_a \frac{di(t)}{dt} + K_e \omega(t) \tag{2.6}$$

Where, $V_a(t)$ is the applied armature voltage, $i(t)$ is the armature current, R_a and L_a are the resistance and inductance of the armature circuit, respectively, and $K_e\omega(t)$ represents the back electromotive force generated due to the rotational motion. The rotational dynamics of the motor shaft are described by Newton's second law for rotational systems [25]:

$$J_a \frac{d\omega(t)}{dt} + B\omega(t) = \tau(t) - \tau_l(t) \tag{2.7}$$

Where, J_a is the equivalent moment of inertia, B is the viscous friction coefficient, $\tau_l(t)$ is the external load torque, and $\tau(t)$ is the electromagnetic torque produced by the motor. The electromagnetic torque is proportional to the armature current and is given by [25]:

$$\tau(t) = K_t i(t) \tag{2.8}$$

The angular position of the motor shaft is related to its angular velocity by [25]:

$$\frac{d\theta(t)}{dt} = \omega(t) \tag{2.9}$$

By combining the electrical and mechanical equations, the complete dynamic behavior of the DC motor can be described. The system clearly shows the coupling between electrical and mechanical domains, where the armature current generates torque, and the rotational motion induces back electromotive force. For control design purposes, the armature inductance L_a is often neglected due to its small effect compared to the electrical and mechanical time constants. Under this assumption, the electrical equation becomes [28]:

$$i(t) = \frac{V_a(t) - K_e\omega(t)}{R_a} \tag{2.10}$$

Substituting this expression into the mechanical equation yields [28]:

$$J_a\frac{d\omega(t)}{dt} + \left(B + \frac{K_tK_e}{R_a}\right)\omega(t) = \frac{K_t}{R_a}V_a(t) - \tau_l(t) \tag{2.11}$$

Finally, the system output is given by [28]:

$$\frac{d\theta(t)}{dt} = \omega(t) \tag{2.12}$$

This reduced-order model is widely used for control system design as it captures the dominant dynamics of the DC motor while simplifying analysis and controller synthesis.

2.5 State-Space Modeling (Single Axis First)

For control system design and analysis, it is convenient to represent the DC motor dynamics in state-space form. This formulation provides a compact representation of the system dynamics and is particularly suitable for modern control techniques such as state feedback, observers, and optimal control. In this section, the state-space model is derived for a single antenna axis. The model is obtained from the reduced-order electromechanical representation of the DC motor, where the armature inductance is neglected due to its relatively small influence on the system dynamics. The mechanical dynamics of the DC motor, including the electrical coupling, are given by:

$$J_a\frac{d\omega(t)}{dt} + \left(B + \frac{K_tK_e}{R_a}\right)\omega(t) = \frac{K_t}{R_a}V_a(t) - \tau_l(t) \tag{2.13}$$

The kinematic relationship between angular position and angular velocity is expressed as follows:

$$\frac{d\theta(t)}{dt} = \omega(t) \tag{2.14}$$

These two equations fully describe the rotational dynamics of the antenna axis. To obtain a state-space representation, the following state variables are defined as follows:

$$x_1(t) = \theta(t) \quad \text{(angular position)} \tag{2.15}$$

$$x_2(t) = \omega(t) \quad \text{(angular velocity)} \tag{2.16}$$

The system input is defined as the armature voltage:

$$u(t) = V_a(t) \tag{2.17}$$

and the external disturbance is the load torque acting on the shaft:

$$d(t) = \tau_l(t) \tag{2.18}$$

Using the definitions above, the system dynamics can be rewritten in first-order form. From the kinematic equation:

$$\dot{x}_1(t) = x_2(t) \tag{2.19}$$

From the mechanical equation:

$$\dot{x}_2(t) = \frac{1}{J_a}\left[\frac{K_t}{R_a}u(t) - \left(B + \frac{K_t K_e}{R_a}\right)x_2(t) - d(t)\right] \tag{2.20}$$

These equations represent the complete dynamic behavior of the single-axis antenna drive system. The controlled output of the system is the angular position of the antenna axis:

$$y(t) = x_1(t) \tag{2.21}$$

The system can now be written in standard state-space form:

$$\dot{x}(t) = Ax(t) + Bu(t) + Ed(t) \tag{2.22}$$

$$y(t) = Cx(t) \tag{2.23}$$

Where the state vector is:

$$x(t) = \begin{bmatrix} x_1(t) \\ x_2(t) \end{bmatrix} = \begin{bmatrix} \theta(t) \\ \omega(t) \end{bmatrix} \tag{2.24}$$

The system matrices are defined as follows:

$$A = \begin{bmatrix} 0 & 1 \\ 0 & -\frac{1}{J_a}\left(B + \frac{K_t K_e}{R_a}\right) \end{bmatrix} \tag{2.25}$$

$$B = \begin{bmatrix} 0 \\ \frac{K_t}{J_a R_a} \end{bmatrix} \tag{2.26}$$

$$E = \begin{bmatrix} 0 \\ -\frac{1}{J_a} \end{bmatrix} \tag{2.27}$$

$$C = \begin{bmatrix} 1 & 0 \end{bmatrix} \tag{2.28}$$

This state-space model provides a complete representation of the single-axis antenna actuator dynamics. The matrix A captures the natural system behavior, including damping effects due to friction and electrical coupling. The matrix B describes how the input voltage influences the system, while the matrix E represents the effect of external disturbances such as wind load or structural resistance. This formulation is particularly useful for controller design, as it allows the application of modern control techniques such as pole placement, LQR design, and observer-based control. In the next section, this single-axis model will be extended to the full two-axis (azimuth and elevation) antenna system.

2.6 Extension to 2-Axis System (AZ/EL)

The deep space antenna tracking system consists of two rotational degrees of freedom corresponding to the azimuth (AZ) and elevation (EL) axes. Each axis is driven by an independent DC motor and is assumed to follow the same electromechanical structure derived in the previous section. Under the decoupling assumption, the interaction between both axes is neglected, meaning that the dynamics of each axis evolve independently. This allows the extension of the single-axis state-space model to a two-axis formulation. The angular positions and velocities of the two axes are defined as follows [29]:

$$\theta_{AZ}(t), \quad \omega_{AZ}(t) = \dot{\theta}_{AZ}(t) \tag{2.29}$$

$$\theta_{EL}(t), \quad \omega_{EL}(t) = \dot{\theta}_{EL}(t) \tag{2.30}$$

Each axis is driven by its corresponding input voltage:

$$u_{AZ}(t) = V_{a,AZ}(t), \quad u_{EL}(t) = V_{a,EL}(t) \tag{2.31}$$

and is subjected to external disturbances (load torques):

$$d_{AZ}(t) = \tau_{l,AZ}(t), \quad d_{EL}(t) = \tau_{l,EL}(t) \tag{2.32}$$

The global state vector of the system is defined as follows [29]:

$$x(t) = \begin{bmatrix} \theta_{AZ}(t) \\ \omega_{AZ}(t) \\ \theta_{EL}(t) \\ \omega_{EL}(t) \end{bmatrix} \tag{2.33}$$

The azimuth axis dynamics are given by [29]:

$$\dot{\theta}_{AZ}(t) = \omega_{AZ}(t) \tag{2.34}$$

$$\dot{\omega}_{AZ}(t) = -\frac{1}{J_{AZ}} \left(B_{AZ} + \frac{K_{t,AZ} K_{e,AZ}}{R_{a,AZ}} \right) \omega_{AZ}(t) + \frac{K_{t,AZ}}{J_{AZ} R_{a,AZ}} u_{AZ}(t) - \frac{1}{J_{AZ}} d_{AZ}(t) \tag{2.35}$$

Similarly, the elevation axis dynamics are [29]:

$$\dot{\theta}_{EL}(t) = \omega_{EL}(t) \tag{2.36}$$

$$\dot{\omega}_{EL}(t) = -\frac{1}{J_{EL}} \left(B_{EL} + \frac{K_{t,EL} K_{e,EL}}{R_{a,EL}} \right) \omega_{EL}(t) + \frac{K_{t,EL}}{J_{EL} R_{a,EL}} u_{EL}(t) - \frac{1}{J_{EL}} d_{EL}(t) \tag{2.37}$$

The complete two-axis system can be written in a compact form [29]:

$$\dot{x}(t) = Ax(t) + Bu(t) + Ed(t) \tag{2.38}$$

$$y(t) = Cx(t) \tag{2.39}$$

Where:

$$u(t) = \begin{bmatrix} u_{AZ}(t) \\ u_{EL}(t) \end{bmatrix}, \quad d(t) = \begin{bmatrix} d_{AZ}(t) \\ d_{EL}(t) \end{bmatrix} \tag{2.40}$$

The system matrices have a block-diagonal structure:

$$A = \begin{bmatrix} A_{AZ} & 0 \\ 0 & A_{EL} \end{bmatrix} \tag{2.41}$$

$$B = \begin{bmatrix} B_{AZ} & 0 \\ 0 & B_{EL} \end{bmatrix}, \quad E = \begin{bmatrix} E_{AZ} & 0 \\ 0 & E_{EL} \end{bmatrix} \tag{2.42}$$

$$C = \begin{bmatrix} 1 & 0 & 0 & 0 \\ 0 & 0 & 1 & 0 \end{bmatrix} \tag{2.43}$$

This formulation represents the complete two-axis antenna tracking system in a unified state-space form. The block-diagonal structure of the system matrices reflects the decoupling

assumption between azimuth and elevation dynamics. This simplifies the controller design process, allowing independent or coordinated control strategies to be applied to each axis depending on system requirements. The developed model serves as the foundation for advanced control techniques such as multivariable control, robust control design, and trajectory tracking for deep space antenna pointing systems. The main objective of a deep space antenna system is to maintain precise alignment with a moving spacecraft. This requires continuously computing the Line-of-Sight (LOS) direction and converting it into azimuth and elevation angles for antenna pointing control. The position of the spacecraft in a global inertial reference frame is defined as follows:

$$\mathbf{r}_s(t) = \begin{bmatrix} x_s(t) \\ y_s(t) \\ z_s(t) \end{bmatrix} \tag{2.44}$$

Similarly, the position of the ground antenna is:

$$\mathbf{r}_a = \begin{bmatrix} x_a \\ y_a \\ z_a \end{bmatrix} \tag{2.45}$$

The Line-of-Sight vector from the antenna to the spacecraft is therefore:

$$\mathbf{r}_{los}(t) = \mathbf{r}_s(t) - \mathbf{r}_a \tag{2.46}$$

The LOS vector is converted into spherical coordinates to obtain the required pointing angles. The azimuth angle is defined as follows:

$$\theta_{ref,AZ}(t) = \tan^{-1}\left(\frac{y_{los}(t)}{x_{los}(t)}\right) \tag{2.47}$$

The elevation angle is defined as follows:

$$\theta_{ref,EL}(t) = \tan^{-1}\left(\frac{z_{los}(t)}{\sqrt{x_{los}^2(t) + y_{los}^2(t)}}\right) \tag{2.48}$$

These angles represent the reference trajectory that the antenna must follow to maintain communication with the spacecraft. The control objective of the antenna system is to minimize the tracking error between the reference LOS angles and the actual antenna angles. The pointing errors for each axis are defined as:

$$e_{AZ}(t) = \theta_{ref,AZ}(t) - \theta_{AZ}(t) \tag{2.49}$$

$$e_{EL}(t) = \theta_{ref,EL}(t) - \theta_{EL}(t) \tag{2.50}$$

In vector form:

$$e(t) = \begin{bmatrix} e_{AZ}(t) \\ e_{EL}(t) \end{bmatrix} = \begin{bmatrix} \theta_{ref,AZ}(t) - \theta_{AZ}(t) \\ \theta_{ref,EL}(t) - \theta_{EL}(t) \end{bmatrix} \tag{2.51}$$

The primary objective of the tracking system is therefore:

$$\lim_{t \to \infty} e(t) = 0 \tag{2.52}$$

This ensures that the antenna axis remains aligned with the spacecraft LOS direction, maintaining stable communication and optimal signal reception. This formulation establishes the direct link between the physical motion of the spacecraft and the control input of the antenna system. The LOS geometry provides the reference trajectory, while the pointing error defines the feedback variable used in controller design. This connection is fundamental for the development of tracking controllers in deep-space communication systems.

2.7 System Constraints

In practical antenna systems, the actuator and mechanical structure are subject to physical limitations and external disturbances. These constraints must be considered to ensure realistic modeling and reliable control system design.

2.7.1 Actuator Saturation

The input voltage applied to the DC motor is limited by the power electronics and supply constraints. This limitation can be expressed as follows [30]:

$$V_{a,\min} \leq V_a(t) \leq V_{a,\max} \tag{2.53}$$

This saturation affects the achievable torque and may lead to performance degradation or nonlinear behavior if not properly handled in the control design.

2.7.2 Angular Velocity Limits

The rotational speed of the antenna axis is bounded due to mechanical and safety constraints [31]:

$$|\omega(t)| \leq \omega_{\max} \tag{2.54}$$

Exceeding this limit may result in structural stress or reduced pointing accuracy.

2.7.3 Acceleration Limits

The angular acceleration is also limited to prevent excessive mechanical stress and to ensure smooth motion [32]:

$$\left| \frac{d\omega(t)}{dt} \right| \leq \alpha_{\max} \tag{2.55}$$

This constraint is particularly important during rapid tracking maneuvers.

2.7.4 Wind Disturbance

External disturbances such as wind forces introduce additional torques acting on the antenna structure. This effect is modeled as a disturbance torque [33]:

$$\tau_l(t) = \tau_{wind}(t) \tag{2.56}$$

where, $\tau_{wind}(t)$ represents time-varying aerodynamic forces. These disturbances can significantly affect pointing accuracy, especially for large reflector antennas.

2.7.5 Mechanical Backlash

Backlash in the gear transmission introduces a dead-zone nonlinearity in the system. Although it is neglected in the primary model for simplicity, its effect can be represented as follows [34]:

$$\theta_{\text{eff}}(t) = \begin{cases} \theta(t) - \Delta, & \text{if } \theta(t) > \Delta \\ 0, & \text{if } |\theta(t)| \leq \Delta \\ \theta(t) + \Delta, & \text{if } \theta(t) < -\Delta \end{cases} \tag{2.57}$$

Where, Δ is the backlash width.

2.8 Conclusion

This chapter has presented a comprehensive mathematical modeling of the deep space antenna system, which serves as the foundation for the control design developed in the following chapters. The antenna was modeled as a two-degree-of-freedom azimuth-elevation (AZ-EL) mechanical structure, with each axis modeled using rigid-body rotational dynamics. The modeling process began by defining the mechanical structure and its degrees of freedom, highlighting the role of azimuth and elevation motions in achieving full spatial tracking capability. The azimuth axis was modeled as a simplified second-order system driven by a DC servo motor, while the elevation axis was modeled as a nonlinear rotational system due to the presence of gravitational torque. In addition, detailed electromechanical models of the DC servo motors were developed for both azimuth and elevation subsystems. A third-order transfer function represented the azimuth drive system, while the elevation subsystem included nonlinear gravitational effects that significantly influence its dynamic behavior.

Coupling effects between the two axes were also discussed and shown to be relatively weak under normal operating conditions. As a result, a decoupled modeling approach was adopted, where each axis is treated as an independent subsystem with bounded interaction effects. In order to facilitate controller design, the nonlinear model was linearized around a nominal operating point, and a unified state-space representation of the system was derived. This representation clearly highlighted the multi-input multi-output (MIMO) structure of the

antenna system and provided a suitable framework for modern control techniques. Finally, external disturbances and uncertainties such as wind loads, friction, structural vibrations, and parameter variations were modeled as additive bounded inputs. These disturbances play a critical role in degrading pointing accuracy and, therefore, must be considered in the controller design. In summary, the developed model provides a realistic and sufficiently accurate representation of the deep space antenna dynamics. It captures the essential physical effects, including inertia, damping, gravitational nonlinearity, and external disturbances. This modeling framework constitutes the basis for the design and implementation of robust control strategies in the next chapter, aimed at achieving high-precision pointing and reliable tracking performance under real operational conditions.

Chapter 3

Control Techniques

3.1 Introduction

The design of accurate and robust control strategies is a critical requirement in deep-space antenna tracking systems. These systems must maintain precise alignment with a moving spacecraft despite the presence of external disturbances, model uncertainties, and nonlinear dynamics. Such constraints make the control problem particularly challenging, especially in high-frequency communication systems where even minor pointing errors can significantly degrade signal quality. Based on the mathematical modeling developed in Chapter 2, the antenna system can be represented as a multi-input multi-output (MIMO) dynamic system consisting of two main subsystems: the azimuth and elevation axes. The azimuth axis is generally characterized by linear second-order dynamics driven by a DC servo motor, while the elevation axis introduces nonlinear behavior due to gravitational torque effects. In addition, both axes are affected by disturbances such as wind loads, friction, and structural vibrations.

In order to address these challenges, this chapter focuses on the design of several control strategies. First, classical linear controllers, including Proportional–Integral (PI), Proportional–Derivative (PD), and Proportional–Integral–Derivative (PID) controllers, are presented. These controllers are widely used in engineering applications due to their simplicity, effectiveness, and ease of implementation. In addition to classical methods, a nonlinear robust control approach, namely Sliding Mode Control (SMC), is also introduced. SMC is known for its strong robustness against parameter uncertainties and external disturbances, making it particularly suitable for nonlinear systems with varying operating conditions. The main objective of this chapter is therefore to develop and analyze PI, PD, PID, and SMC controllers for the antenna system, and to evaluate their performance in terms of tracking accuracy, stability, and robustness. This provides a solid foundation for the subsequent chapter, where optimization techniques will be applied to further enhance controller performance.

3.2 Proportional-Integral (PI) Controller

The Proportional-Integral (PI) controller is a widely used feedback control strategy due to its simplicity and its ability to eliminate steady-state error. It combines proportional action, which reacts to the current system behavior, with integral action, which accumulates past

information to improve long-term accuracy. The PI controller is commonly used in systems where steady-state precision is more critical than fast transient response [35].

3.2.1 Control Law

The PI control law is expressed as follows [35]:

$$u(t) = K_p e(t) + K_i \int_0^t e(\tau)\, d\tau \tag{3.1}$$

Where:

- K_p is the proportional gain,
- K_i is the integral gain,
- $u(t)$ is the control signal applied to the system.

3.2.2 Closed-Loop PI Control Structure

The PI controller is implemented in a closed-loop feedback configuration to ensure continuous correction of the system output. The general structure is shown in Figure 3.1 [36].

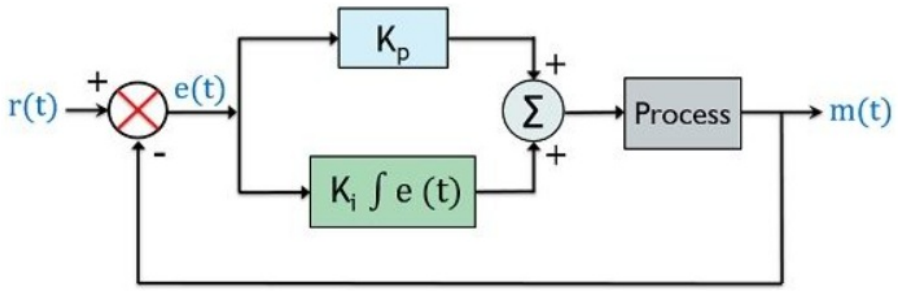


Figure 3.1: Closed-loop structure of a PI control system

In this configuration, the system output is continuously compared to the reference input, and the controller adjusts the control signal to reduce the deviation over time.

3.2.3 Transfer Function Representation

In the Laplace domain, the PI controller is represented as follows [35]:

$$C(s) = K_p + \frac{K_i}{s} \tag{3.2}$$

The Equation 3.2 can be represented in the equivalent form as follows [35]:

$$C(s) = \frac{K_p s + K_i}{s} \tag{3.3}$$

3.2.4 Role of Each Term

The PI controller consists of two complementary actions [35]:

- **Proportional action:** improves the transient response by reacting to current system behavior.
- **Integral action:** eliminates steady-state error by accumulating past errors.

3.2.5 Advantages

- Eliminates steady-state error,
- Simple structure and easy implementation,
- Robust performance for slow and moderate systems,
- Effective against constant disturbances.

3.2.6 Limitations

- Slower transient response compared to PD or PID controllers,
- Possible overshoot due to integral accumulation,
- Limited performance in highly dynamic systems.

3.2.7 Remarks

The PI controller is widely used as a baseline control strategy due to its simplicity and ability to ensure steady-state accuracy. However, its performance depends strongly on proper tuning of its gains, which motivates the use of systematic tuning methods and optimization techniques in the following sections.

3.3 Proportional-Derivative (PD) Controller

The Proportional-Derivative (PD) controller is a classical feedback control strategy used to improve the dynamic response of control systems. It combines proportional action, which reacts to the current system behavior, with derivative action, which provides a predictive effect based on the rate of change of the system output. This makes the PD controller particularly effective in improving transient performance and enhancing system stability [35].

3.3.1 Control Law

The PD control law is expressed as follows [35]:

$$u(t) = K_p e(t) + K_d \frac{de(t)}{dt} \tag{3.4}$$

Where:

- K_p is the proportional gain,
- K_d is the derivative gain,
- $u(t)$ is the control signal applied to the system.

3.3.2 Closed-Loop PD Control Structure

The PD controller is implemented in a closed-loop feedback configuration to ensure continuous correction of the system output. The general structure is shown in Figure 3.2 [36].

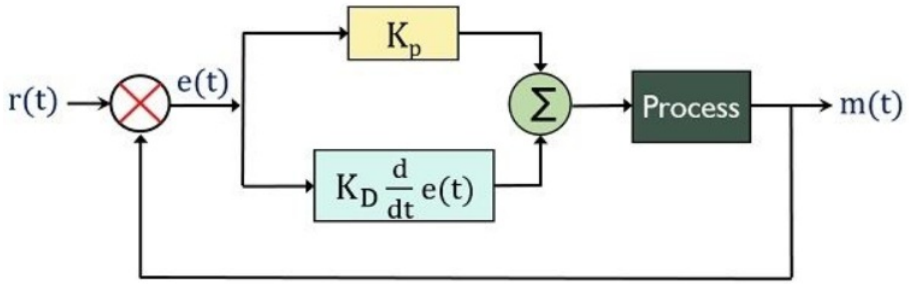


Figure 3.2: Closed-loop structure of a PD control system

In this configuration, the system output is continuously compared with the reference input, and the controller generates a corrective signal based on both the magnitude and the rate of change of the deviation.

3.3.3 Transfer Function Representation

In the Laplace domain, the PD controller is represented as follows [35]:

$$C(s) = K_p + K_d s \tag{3.5}$$

3.3.4 Role of Each Term

The PD controller consists of two main components:

- **Proportional action:** improves response speed by reacting to the current system behavior.
- **Derivative action:** enhances damping by anticipating future system trends and reducing oscillations.

3.3.5 Advantages

- Improved transient response,
- Reduced overshoot and oscillations,
- Increased system damping,
- Simple implementation with low computational cost.

3.3.6 Limitations

- Does not eliminate steady-state error,
- Sensitive to measurement noise due to derivative action,
- Performance depends on proper tuning of gains.

3.3.7 Remarks

The PD controller is mainly used to improve the dynamic behavior of control systems by enhancing damping and stability. However, due to its inability to eliminate steady-state error, it is often combined with integral action in more advanced control structures.

3.4 Proportional-Integral-Derivative (PID) Controller

The Proportional-Integral-Derivative (PID) controller is the most widely used feedback control structure in industrial and engineering applications. It combines the advantages of proportional, integral, and derivative actions to achieve a balanced trade-off between fast transient response, accurate steady-state performance, and improved stability. The PID controller is considered a general extension of both PI and PD controllers and is often used as a baseline controller for a wide range of dynamic systems [35].

3.4.1 Control Law

The PID control law is expressed as follows [35]:

$$u(t) = K_p e(t) + K_i \int_0^t e(\tau)\, d\tau + K_d \frac{de(t)}{dt} \tag{3.6}$$

Where:

- K_p is the proportional gain,
- K_i is the integral gain,
- K_d is the derivative gain,
- $u(t)$ is the control signal applied to the system.

3.4.2 Closed-Loop PID Control Structure

The PID controller is typically implemented in a closed-loop configuration to ensure feedback regulation and disturbance rejection. The general structure is shown in Figure 3.3 [36].

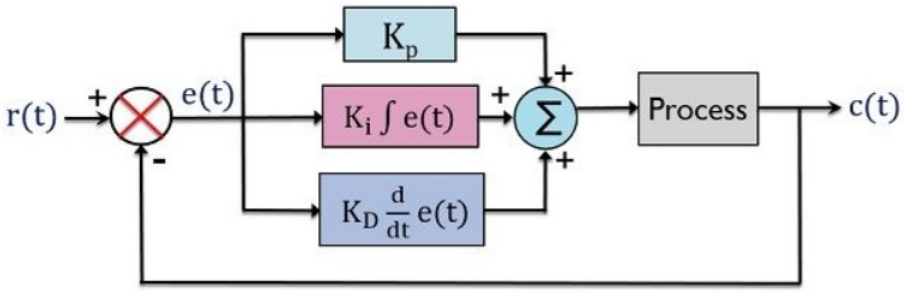


Figure 3.3: Closed-loop structure of a PID control system

This configuration ensures that the system output is continuously compared with the reference input, and the control signal is adjusted accordingly to minimize the deviation.

3.4.3 Transfer Function Representation

In the Laplace domain, the PID controller is represented as follows:

$$C(s) = K_p + \frac{K_i}{s} + K_d s \tag{3.7}$$

The same as previously, the Equation 3.7 can be represented in the equivalent form as follows:

$$C(s) = \frac{K_d s^2 + K_p s + K_i}{s} \tag{3.8}$$

3.4.4 Role of Each Term

The PID controller consists of three complementary actions:

- **Proportional action:** improves response speed and reduces overall deviation.
- **Integral action:** eliminates steady-state error by accumulating past system behavior.
- **Derivative action:** improves damping and reduces overshoot by predicting future trends.

3.4.5 Advantages

- Good balance between transient and steady-state performance,
- Wide applicability to linear and weakly nonlinear systems,
- Simple structure and ease of implementation,
- Improved robustness compared to PI and PD controllers.

3.4.6 Limitations

- Requires proper tuning of three parameters,
- Sensitive to measurement noise, especially in the derivative term,
- Performance may degrade in highly nonlinear systems,
- Possible overshoot if not properly tuned.

3.4.7 Remarks

The PID controller is widely adopted due to its simplicity and effectiveness. However, its performance strongly depends on the appropriate tuning of its gains, which motivates the use of systematic tuning methods and optimization algorithms in the following sections.

3.5 Sliding Mode Control (SMC)

Sliding Mode Control (SMC) is a robust nonlinear control technique widely used for systems operating under uncertainties, external disturbances, and parameter variations. The main idea of SMC is to force the system trajectories to reach a predefined surface, called the sliding surface (Figure 4.2 [37]), and maintain the motion on this surface regardless of disturbances and model uncertainties. The main advantage of SMC is its robustness property, which ensures that the closed-loop system becomes insensitive to matched uncertainties once the sliding mode is reached [38].

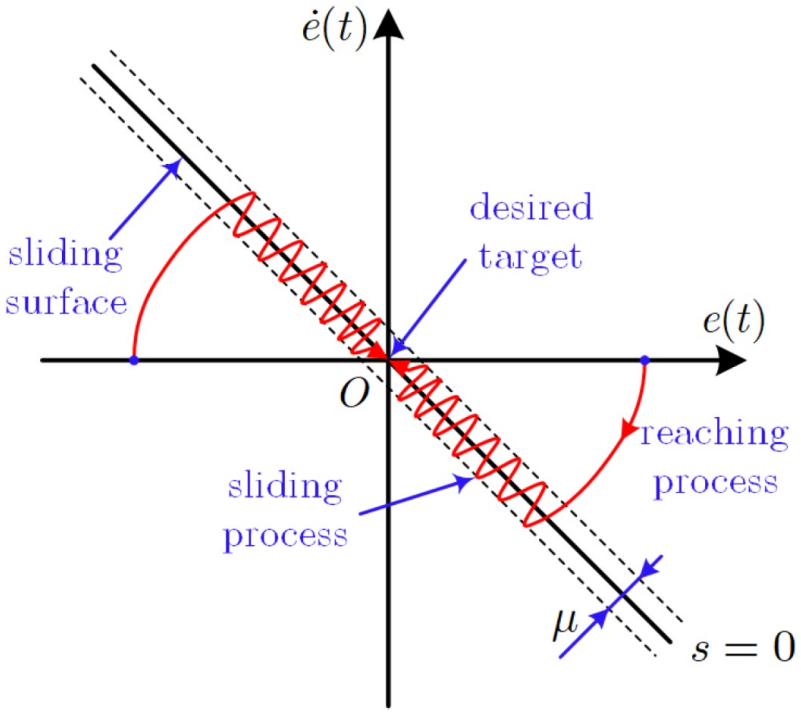


Figure 3.4: SMC sliding surface

3.5.1 System Description

Consider a general nonlinear system described by [38]:

$$\dot{x}(t) = f(x,t) + g(x,t)u(t) + d(t) \tag{3.9}$$

Where:

- $x(t)$ is the state vector,
- $u(t)$ is the control input,
- $f(x,t)$ represents the nominal system dynamics,
- $g(x,t)$ is the input gain,
- $d(t)$ represents external disturbances and uncertainties.

The objective is to design a control law $u(t)$ such that the system output follows a desired reference trajectory.

3.5.2 Sliding Surface Design

The sliding surface is designed to define the desired error dynamics. A common form for first-order systems is given as follows:

$$s(t) = \dot{e}(t) + \lambda e(t) \tag{3.10}$$

Where:

- $e(t)$ is the tracking error,
- $\lambda > 0$ is a design parameter that determines the convergence rate.

A more general form for higher-order systems is given by [17]:

$$s = \left(\frac{d}{dt} + \lambda\right)^{n-1} e \tag{3.11}$$

Where:

- s is the sliding surface,
- e is the system error,
- n is the relative degree of the system,
- $\lambda > 0$ is a positive parameter that defines the convergence speed on the sliding manifold.

When $s(t) = 0$, the system dynamics are reduced to a stable lower-order system.

3.5.3 SMC Control Law

The sliding mode control law is composed of two parts [17]:

$$u(t) = u_{eq}(t) + u_{sw}(t) \tag{3.12}$$

Where, $u_{eq}(t)$ is the equivalent control and $u_{sw}(t)$ is the switching control.

3.5.3.1 Equivalent Control

The equivalent control maintains the system motion on the sliding surface. It is obtained by enforcing the condition [17]:

$$\dot{s}(x,t) = 0 \tag{3.13}$$

This leads to the following [17]:

$$u_{eq}(t) = -\frac{f(x,t) + \lambda \dot{e}(t)}{g(x,t)} \tag{3.14}$$

The equivalent control ensures that once the sliding mode is reached, the system follows the desired reduced-order dynamics.

3.5.3.2 Switching Control

The switching control is responsible for driving the system trajectories toward the sliding surface. It is defined as follows [17]:

$$u_{sw}(t) = -K \operatorname{sign}(s) \tag{3.15}$$

Where, $K > 0$ is a positive gain selected to overcome disturbances and uncertainties. In order to reduce the chattering effect, the discontinuous function can be approximated using a boundary layer approach [39]:

$$\operatorname{sign}(s) \approx \operatorname{sat}\left(\frac{s}{\phi}\right) \tag{3.16}$$

Where, $\phi > 0$ defines the boundary layer thickness.

3.5.4 Reaching Condition

In order to ensure convergence toward the sliding surface, the following condition must be satisfied [40]:

$$s(t)\dot{s}(t) < 0 \tag{3.17}$$

This condition guarantees that the system trajectories are always directed toward the sliding manifold.

3.5.5 Advantages and Limitations

Advantages

- High robustness against parameter uncertainties and disturbances,
- Fast convergence to the desired dynamics,
- Simple control structure,
- Strong stability properties based on Lyapunov theory.

Limitations

- Chattering phenomenon due to discontinuous control action,
- Requires knowledge of system structure,
- High control effort in switching term,
- Sensitivity to measurement noise.

3.6 Conclusion

In this chapter, several control strategies have been developed and analyzed for the regulation of dynamic systems. Classical linear controllers, including PI, PD, and PID, were first presented due to their simplicity, ease of implementation, and effectiveness in a wide range of engineering applications. These controllers provide satisfactory performance for systems with relatively simple dynamics; however, their effectiveness may be limited in the presence of nonlinearities and external disturbances. In order to overcome these limitations, a nonlinear robust control approach based on Sliding Mode Control (SMC) was introduced. Unlike classical controllers, SMC offers strong robustness against parameter uncertainties and disturbances by forcing the system trajectories to converge to a predefined sliding surface. This property makes it particularly suitable for systems operating under uncertain or varying conditions.

The analysis of these control techniques highlights the trade-off between simplicity and performance. While PI, PD, and PID controllers are straightforward to design and implement, their performance strongly depends on appropriate parameter tuning. In contrast, SMC provides enhanced robustness and stability but may introduce practical challenges such as chattering. Overall, this chapter establishes a solid foundation for control system design by presenting both classical and advanced approaches. In the following chapter, optimization techniques will be employed to determine optimal controller parameters and improve system performance. Furthermore, a comparative analysis of the different controllers and tuning methods will be conducted in subsequent chapters in order to evaluate their effectiveness in terms of accuracy, robustness, and dynamic response.

Chapter 4

Tuning and Optimization Techniques

4.1 Introduction

The design of efficient control systems relies heavily on the appropriate tuning of controller parameters to achieve desired performance in terms of stability, accuracy, and robustness. In classical control engineering, Proportional–Integral–Derivative (PID) controllers remain among the most widely used strategies due to their simple structure and ease of implementation. However, the performance of PID controllers strongly depends on the selection of their tuning parameters, which has motivated the development of various tuning methodologies. Among these, empirical approaches such as the Ziegler–Nichols (ZN) method have been extensively adopted as practical solutions for obtaining initial controller settings without requiring an accurate mathematical model of the system. Despite their simplicity and effectiveness in many applications, such classical tuning methods often lead to aggressive responses, including overshoot and oscillations, especially when dealing with nonlinear or highly dynamic systems. In order to overcome these limitations, advanced control strategies such as Sliding Mode Control (SMC) have been introduced, offering enhanced robustness against uncertainties, disturbances, and parameter variations. Nevertheless, SMC design also involves critical parameter selection, which directly influences system performance and phenomena such as chattering.

In recent years, metaheuristic optimization techniques have emerged as powerful tools for addressing complex tuning problems in control systems. Algorithms such as Particle Swarm Optimization (PSO), Grey Wolf Optimization (GWO), and Ant Colony Optimization (ACO) provide efficient search mechanisms capable of exploring nonlinear and multimodal solution spaces without relying on gradient information. These methods enable the automatic tuning of controller parameters to achieve improved dynamic performance and robustness compared to conventional approaches. This chapter presents a comprehensive review of both classical and modern tuning techniques. It begins with the Ziegler–Nichols method and its variants, followed by an overview of advanced control strategies and metaheuristic optimization algorithms. The objective is to establish a solid theoretical foundation for the development and optimization of control systems, which will be further explored and evaluated in the subsequent chapters.

4.1.1 Ziegler–Nichols Tuning Method

Among the classical techniques used for tuning proportional (P), proportional–integral (PI), and proportional–integral–derivative (PID) controllers, the Ziegler–Nichols (ZN) method is one of the most established and widely adopted approaches. Introduced by Ziegler and Nichols in 1942, this method is based on empirical observations of system behavior combined with the structure of feedback control systems. The ZN approach provides practical tuning rules that allow the determination of controller parameters without requiring an exact mathematical model of the system. Several variants exist, including closed-loop (ultimate gain) tuning, open-loop (step response) tuning, and frequency-based tuning methods. These approaches aim to achieve acceptable transient performance and stability margins [41].

4.1.1.1 Ultimate Gain Method

In the ultimate gain method, the system is first operated using only proportional control. The proportional gain is gradually increased until the closed-loop system reaches the verge of instability, where sustained oscillations occur. The gain at this operating point is called the ultimate gain K_u, while the corresponding oscillation period is referred to as the ultimate period T_u. These two parameters are then used to compute the controller settings. The Ziegler–Nichols tuning rules derived from this method provide initial values for P, PI, PD, and PID controllers. Although these settings typically result in fast system response, they may also introduce overshoot and oscillatory behavior [7].

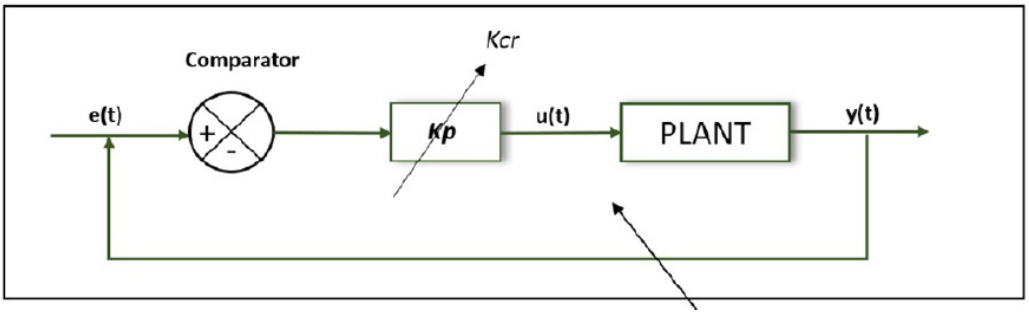


Figure 4.1: Closed-loop ultimate gain tuning procedure

Table 4.1: Ziegler–Nichols tuning rules based on the ultimate gain method.

Controller Type	Tuning Parameters
P	$K_p = 0.5K_u$
PI	$K_p = 0.45K_u, \quad K_i = \frac{1.2K_p}{T_u}$
PD	$K_p = 0.8K_u, \quad K_d = 0.1K_uT_u$
PID	$K_p = 0.6K_u, \quad K_i = \frac{1.2K_p}{T_u}, \quad K_d = 0.075K_uT_u$

4.1.1.2 Step Response Method

The step response method is an open-loop tuning technique based on analyzing the system's reaction to a step input. The resulting response, known as the process reaction curve, is used to extract key dynamic characteristics of the system. A tangent line is drawn at the point of maximum slope of the response curve. The intersection of this tangent with the time axis defines the apparent delay, while the slope of the response provides information about the system dynamics. These values are then used to compute controller parameters [7].

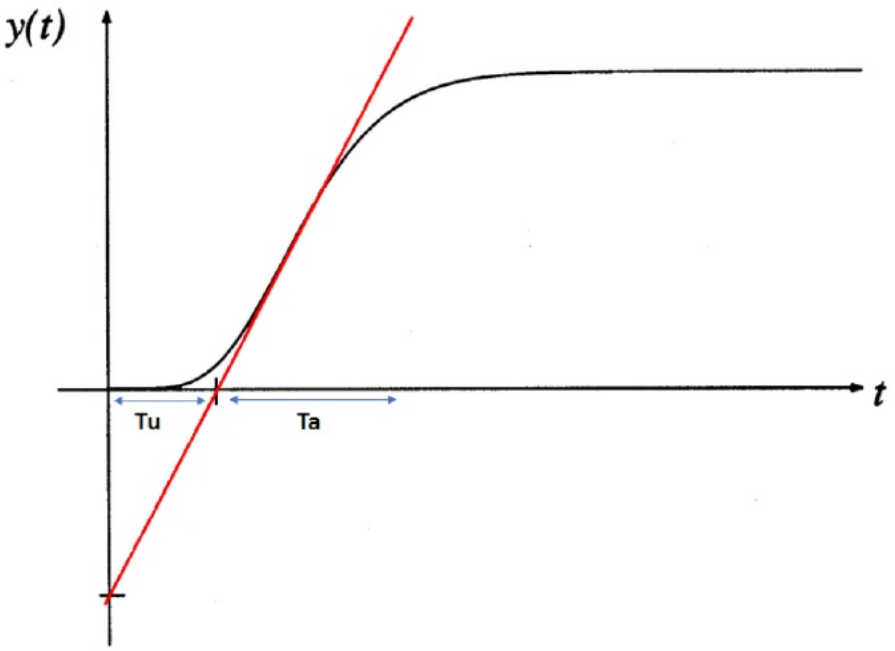


Figure 4.2: Open-loop step response tuning procedure

Table 4.2: Ziegler–Nichols tuning rules based on the step response method.

Controller Type	Tuning Parameters
P	$K_p = 1.2\frac{T_a}{T_u}$
PI	$K_p = 1.2\frac{T_a}{T_u}, \quad T_i = 2T_u$
PID	$K_p = 1.2\frac{T_a}{T_u}, \quad T_i = 2T_u, \quad T_d = 0.5T_u$

4.1.1.3 Advantages and Limitations of the ZN Method

The Ziegler–Nichols method is widely used due to its simplicity and ease of implementation. However, it represents a compromise between simplicity and performance quality. While it provides quick initial tuning values, further refinement is often required in practical applications [42].

Advantages

- Simple and easy to apply in both simulation and experimental environments.
- Does not require an accurate mathematical model of the system.
- Provides fast initial estimates for controller parameters.
- Applicable to P, PI, PD, and PID controllers.

Limitations

- May produce aggressive control actions with overshoot.
- Can lead to oscillatory system behavior.
- Requires operation near the stability limit, which may not be safe in practice.
- Limited performance for nonlinear or highly sensitive systems.

4.2 Metaheuristic Optimization Techniques

Metaheuristic optimization methods have become essential tools in engineering and control applications for solving complex, nonlinear, and multimodal optimization problems. Unlike traditional optimization approaches, these techniques do not rely on gradient information and are capable of exploring the search space more effectively, reducing the risk of being trapped in local optima. This makes them particularly suitable for tuning controller parameters in nonlinear systems. Most metaheuristic algorithms are inspired by natural processes, such as biological evolution, collective behavior of social organisms, or physical phenomena [43].

4.2.1 Particle Swarm Optimization (PSO)

Particle Swarm Optimization (PSO) is a population-based optimization algorithm inspired by the collective behavior observed in bird flocks and fish schools. It has been widely applied to solve complex optimization problems where conventional techniques may not be effective. In PSO, a set of particles moves through the search space, where each particle represents a potential solution. These particles iteratively update their positions based on both their individual experience and the collective knowledge of the swarm in order to converge toward the optimal solution [43]. Let the i-th particle in an n-dimensional search space be defined by its position vector:

$$\mathbf{x}_i = [x_{i1}, x_{i2}, \ldots, x_{in}]^T \tag{4.1}$$

And its velocity vector:

$$\mathbf{v}_i = [v_{i1}, v_{i2}, \ldots, v_{in}]^T. \tag{4.2}$$

The movement of each particle is governed by updating its velocity and position according to the following equations:

$$\mathbf{v}_i(t+1) = w\mathbf{v}_i(t) + c_1 r_1(\mathbf{pbest}_i - \mathbf{x}_i(t)) + c_2 r_2(\mathbf{gbest} - \mathbf{x}_i(t)) \tag{4.3}$$

$$\mathbf{x}_i(t+1) = \mathbf{x}_i(t) + \mathbf{v}_i(t+1) \tag{4.4}$$

Where, w denotes the inertia weight controlling the influence of the previous velocity, c_1 and c_2 are acceleration coefficients associated with cognitive and social components, and r_1, r_2 are random variables uniformly distributed in the interval $[0, 1]$. The term $\mathbf{pbest}_i$ represents the best position previously visited by the i-th particle, while **gbest** corresponds to the best solution found by the entire swarm [43]. At each iteration, a fitness function $f(\mathbf{x}_i)$ is evaluated for every particle. The personal best and global best positions are updated according to:

$$\mathbf{pbest}_i(t+1) = \begin{cases} \mathbf{x}_i(t), & \text{if } f(\mathbf{x}_i(t)) < f(\mathbf{pbest}_i(t)) \\ \mathbf{pbest}_i(t), & \text{otherwise} \end{cases} \tag{4.5}$$

$$\mathbf{gbest}(t+1) = \arg\min_i f(\mathbf{pbest}_i(t+1)) \tag{4.6}$$

In order to ensure numerical stability and prevent excessive movement of particles, velocity limits are often imposed:

$$v_{ij}^{\min} \leq v_{ij}(t) \leq v_{ij}^{\max}, \quad j = 1, 2, \ldots, n \tag{4.7}$$

The algorithm continues iterating until a predefined stopping condition is satisfied, such as reaching a maximum number of iterations, achieving a desired fitness value, or observing negligible improvement in the global best solution. The behavior of particles within the search space is illustrated in Figure 4.3, where each particle is influenced by both its own best position and the swarm's global best. Additionally, the overall procedure of the PSO algorithm is summarized in the flowchart shown in Figure 4.4 [43].

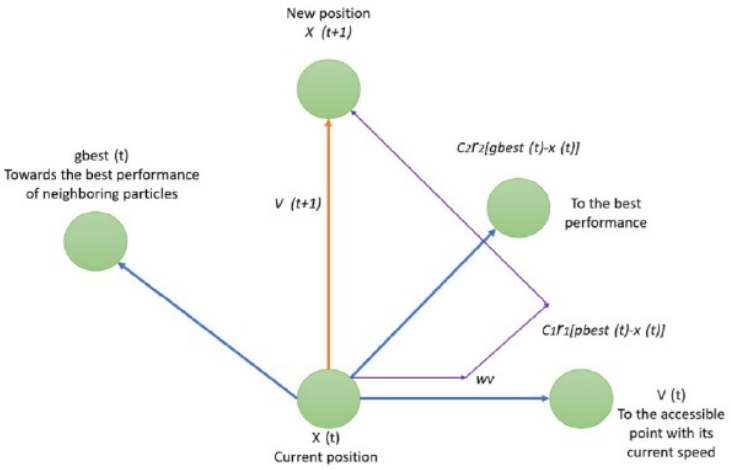


Figure 4.3: PSO particle movement in the search space

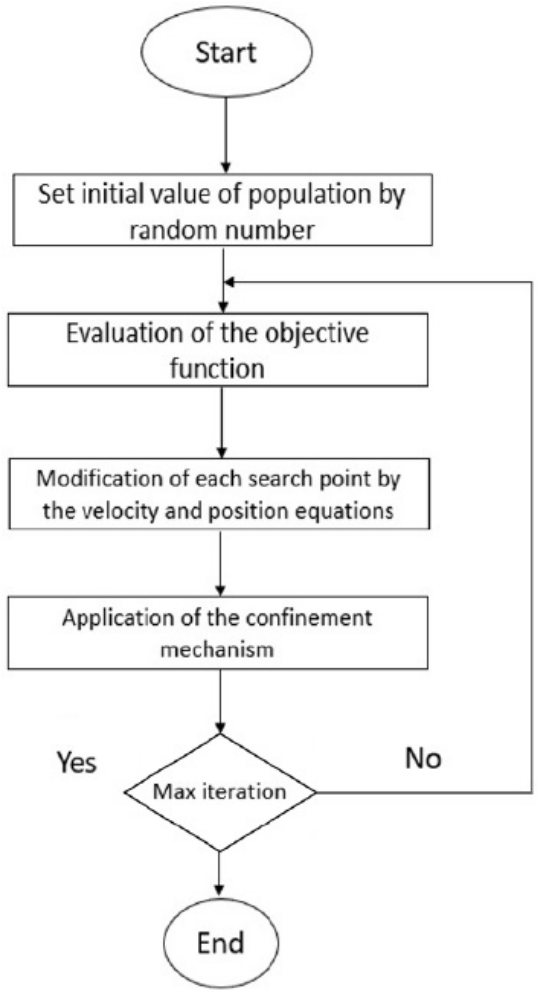


Figure 4.4: Flowchart of the PSO algorithm

4.2.2 Grey Wolf Optimization (GWO)

Grey Wolf Optimization (GWO) is a nature-inspired metaheuristic algorithm that mimics the leadership hierarchy and cooperative hunting behavior of grey wolves in nature. The method models the social organization of wolves and their coordinated strategy for locating and capturing prey, making it effective for solving complex optimization problems [44]. In GWO, the population of candidate solutions is divided into four hierarchical levels: alpha (α), beta (β), delta (δ), and omega (ω). The first three categories represent the best solutions found so far and guide the search process, while the remaining wolves follow their guidance to explore the search space [44]. The optimization process is conceptually divided into three main stages:

- Encircling the prey (exploration of the search space),
- Hunting (exploitation guided by the best solutions),
- Attacking the prey (convergence toward the optimum).

4.2.2.1 Social Hierarchy

The best solution obtained during the search is designated as α, followed by the second and third best solutions, β and δ, respectively. All remaining candidate solutions are categorized as ω. This hierarchical structure ensures that the search process is directed by the most promising solutions.

4.2.2.2 Encircling Behavior

The encircling mechanism represents the ability of wolves to estimate the position of the prey and move toward it. This behavior is modeled mathematically as follows [44]:

$$\overrightarrow{D} = \left| \overrightarrow{C}\, \overrightarrow{X_p}(t) - \overrightarrow{X}(t) \right| \tag{4.8}$$

$$\overrightarrow{X}(t+1) = \overrightarrow{X_p}(t) - \overrightarrow{A}\, \overrightarrow{D} \tag{4.9}$$

Where, $\overrightarrow{X_p}$ represents the position of the prey (best solution), $\overrightarrow{X}$ is the current position of a wolf, and t denotes the iteration index. The coefficient vectors $\overrightarrow{A}$ and $\overrightarrow{C}$ are defined as follows [44]:

$$\overrightarrow{A} = 2a\, \overrightarrow{r}_2 - a, \quad \overrightarrow{C} = 2\, \overrightarrow{r}_1 \tag{4.10}$$

Where, a is a control parameter that decreases linearly from 2 to 0 over iterations, and $\overrightarrow{r}_1, \overrightarrow{r}_2$ are random vectors in the range $[0, 1]$.

4.2.2.3 Hunting Mechanism

The hunting phase is guided by the three best solutions (α, β, and δ). The positions of the wolves are updated based on these leaders as follows [44]:

$$\overrightarrow{D_\alpha} = \left| \overrightarrow{C_1}\, \overrightarrow{X_\alpha}(t) - \overrightarrow{X}(t) \right| \tag{4.11}$$

$$\overrightarrow{D_\beta} = \left| \overrightarrow{C_2}\, \overrightarrow{X_\beta}(t) - \overrightarrow{X}(t) \right| \tag{4.12}$$

$$\overrightarrow{D_\delta} = \left| \overrightarrow{C_3}\, \overrightarrow{X_\delta}(t) - \overrightarrow{X}(t) \right| \tag{4.13}$$

The candidate positions influenced by each leader are computed as follows [44]:

$$\overrightarrow{X_1} = \overrightarrow{X_\alpha} - \overrightarrow{A_1}\overrightarrow{D_\alpha} \tag{4.14}$$

$$\overrightarrow{X_2} = \overrightarrow{X_\beta} - \overrightarrow{A_2}\overrightarrow{D_\beta} \tag{4.15}$$

$$\overrightarrow{X_3} = \overrightarrow{X_\delta} - \overrightarrow{A_3}\overrightarrow{D_\delta} \tag{4.16}$$

Finally, the updated position of each wolf is obtained by averaging these contributions [44]:

$$\overrightarrow{X}(t+1) = \frac{\overrightarrow{X_1} + \overrightarrow{X_2} + \overrightarrow{X_3}}{3} \tag{4.17}$$

4.2.2.4 Attacking the Prey

The convergence toward the optimal solution is achieved by gradually reducing the parameter a, which decreases the magnitude of $\overrightarrow{A}$. As $|\overrightarrow{A}|$ becomes smaller than 1, the wolves move closer to the prey, refining their search and focusing on exploitation. The position update mechanism and the influence of the coefficient $\overrightarrow{A}$ are illustrated in Figure 4.5, while the overall algorithmic procedure is summarized in the flowchart shown in Figure 4.6.

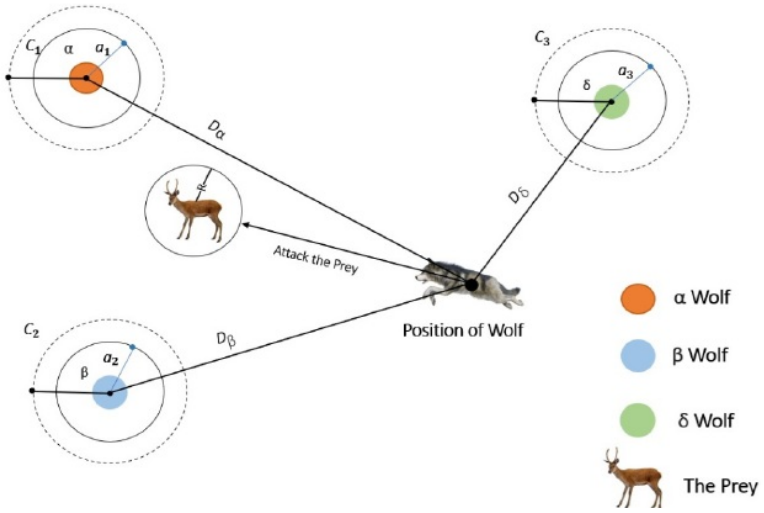


Figure 4.5: Position updating mechanism of grey wolves and the effect of coefficient $\overrightarrow{A}$

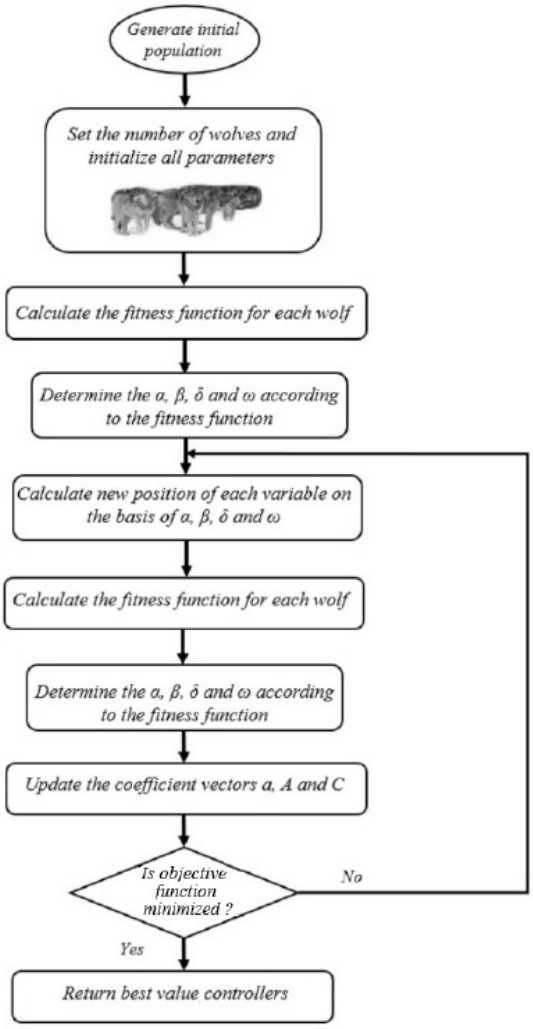


Figure 4.6: Flowchart of the GWO algorithm

4.2.3 Ant Colony Optimization (ACO)

Ant Colony Optimization (ACO) is a population-based metaheuristic inspired by the foraging behavior of real ants. It was originally proposed to solve combinatorial optimization problems and has since been extended to continuous optimization domains. The fundamental idea behind ACO is the indirect communication between ants through pheromone trails, which allows them to collectively find optimal paths. In nature, ants deposit pheromones along their paths when searching for food. Over time, shorter or more efficient paths accumulate higher pheromone concentrations, attracting more ants and reinforcing the optimal solution. This collective behavior is modeled in ACO to solve optimization problems [45].

4.2.3.1 Solution Construction

In ACO, each artificial ant incrementally constructs a solution by moving through the search space. The decision of selecting the next component of the solution is based on a probabilistic rule that depends on pheromone intensity and heuristic information. The probability of choosing a solution component is given by [45]:

$$P_{ij}^{k}(t) = \frac{\left[\tau_{ij}(t)\right]^{\alpha}\left[\eta_{ij}\right]^{\beta}}{\sum_{j\in\mathcal{N}_i}\left[\tau_{ij}(t)\right]^{\alpha}\left[\eta_{ij}\right]^{\beta}} \tag{4.18}$$

Where:

- $\tau_{ij}(t)$ is the pheromone intensity on path (i, j) at iteration t,
- η_{ij} is the heuristic desirability of choosing path (i, j),
- α controls the influence of pheromone trails,
- β controls the influence of heuristic information,
- $\mathcal{N}_i$ is the set of feasible moves from node i.

4.2.3.2 Pheromone Update

After all ants construct their solutions, the pheromone trails are updated to reinforce good solutions and reduce the influence of poor ones. The update rule is defined as follows [45]:

$$\tau_{ij}(t+1) = (1-\rho)\tau_{ij}(t) + \Delta\tau_{ij}(t) \tag{4.19}$$

Where:

- $\rho \in (0, 1)$ is the evaporation rate,
- $\Delta\tau_{ij}(t)$ represents the pheromone deposited by ants.

The pheromone deposit is computed as follows [45]:

$$\Delta\tau_{ij}(t) = \sum_{k=1}^{N}\Delta\tau_{ij}^{k}(t) \tag{4.20}$$

$$\Delta\tau_{ij}^{k}(t) = \begin{cases} \frac{Q}{L_k}, & \text{if ant } k \text{ uses path } (i, j) \\ 0, & \text{otherwise} \end{cases} \tag{4.21}$$

Where:

- Q is a constant,
- L_k is the cost (or fitness) of the solution constructed by ant k.

4.2.3.3 Exploration and Exploitation

ACO balances exploration and exploitation through the parameters α, β, and ρ. A higher pheromone influence encourages exploitation of known good solutions, while a stronger heuristic influence promotes exploration of new regions in the search space.

4.2.3.4 Algorithm Procedure

The general steps of the ACO algorithm are summarized as follows:

1. Initialize pheromone levels.
2. Construct solutions using probabilistic rules.
3. Evaluate the fitness of each solution.
4. Update pheromone trails.
5. Repeat until a stopping criterion is satisfied.

The behavior of ants and pheromone trail formation is illustrated in Figure 4.7, where shorter paths accumulate higher pheromone concentration over time.

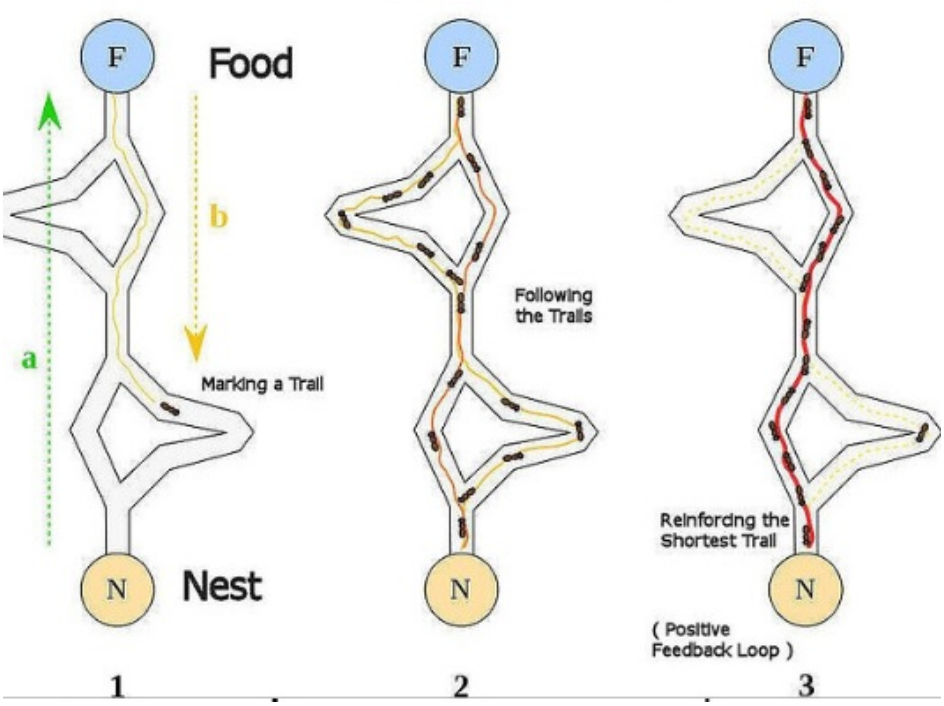


Figure 4.7: Illustration of ant movement and pheromone trail formation

The overall process of the ACO algorithm is shown in the flowchart in Figure 4.8, summarizing the iterative optimization procedure [46].

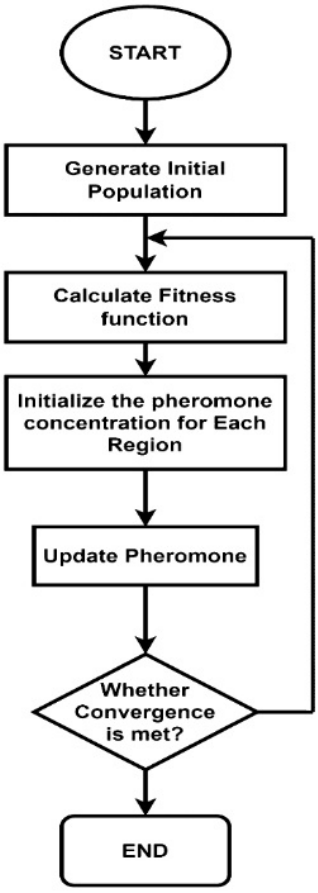


Figure 4.8: Flowchart of the Ant Colony Optimization algorithm

4.3 Conclusion

This chapter has presented a comprehensive overview of controller tuning and optimization techniques. Classical tuning methods, such as the Ziegler–Nichols approach, were first discussed as practical tools for determining initial parameters of P, PI, PD, and PID controllers. Although simple to apply, these methods may lead to oscillatory responses and often require further refinement to satisfy performance requirements. In addition to conventional techniques, advanced control strategies such as Sliding Mode Control (SMC) were introduced. SMC offers strong robustness against parameter uncertainties and external disturbances, making it particularly suitable for nonlinear systems. Its ability to ensure stable system behavior under varying conditions represents a significant advantage over classical linear controllers, despite challenges such as chattering.

Furthermore, modern metaheuristic optimization algorithms, including Particle Swarm Optimization (PSO), Grey Wolf Optimization (GWO), and Ant Colony Optimization (ACO), were investigated. These techniques provide efficient solutions for tuning controller parameters in complex systems, as they do not rely on gradient information and are capable of escaping local optima. Each method exhibits distinct characteristics: PSO is known for its simplicity and rapid convergence, GWO offers a balanced exploration-exploitation mechanism inspired by social hierarchy, and ACO relies on collective learning through pheromone-

based interactions. Overall, the integration of advanced control strategies and metaheuristic optimization techniques provides a powerful framework for improving system performance in terms of stability, accuracy, and robustness. The concepts developed in this chapter serve as a foundation for the subsequent chapter, where these methods will be applied and evaluated through simulation and comparative analysis.

Chapter 5

Results and Discussion

5.1 Introduction

This chapter presents and analyzes the performance of the proposed control strategies applied to the two-axis (azimuth–elevation) antenna tracking system. The objective is to evaluate and compare different control approaches in terms of tracking accuracy, robustness, and overall dynamic response under identical operating conditions. In order to achieve this end, several controllers are implemented and tested. First, classical Proportional–Integral–Derivative (PID) controllers optimized using Ziegler–Nichols (ZN) and different metaheuristic algorithms are considered, namely Particle Swarm Optimization (PSO-PID), Grey Wolf Optimization (GWO-PID), and Ant Colony Optimization (ACO-PID). These methods aim to determine optimal controller gains by minimizing the Integral of Time-weighted Absolute Error (ITAE), ensuring fast response and reduced steady-state error.

In addition, a nonlinear Sliding Mode Control (SMC) strategy optimized via Ant Colony Optimization (ACO-SMC) is introduced to enhance system robustness against disturbances and model uncertainties. Finally, a hybrid control scheme combining PID and SMC actions (ACO-SMC-PID) is proposed, where the PID component ensures smooth tracking performance while the SMC term improves robustness and disturbance rejection. All controllers are evaluated using the same system model, reference trajectories derived from the Line-of-Sight (LOS) tracking requirement, and identical simulation conditions. The comparison is carried out based on several performance criteria, including tracking accuracy, transient response characteristics, control effort, and ITAE values. The results presented in this chapter highlight the strengths and limitations of each control approach and demonstrate the effectiveness of the proposed hybrid ACO-SMC-PID controller in achieving a superior balance between performance and robustness for deep-space antenna tracking applications.

5.2 Results Analysis

In this section, metaheuristic optimization algorithms, ACO, GWO, PSO, and the classical ZN are employed to optimally tune the parameters of PID, SMC, and hybrid SMC-PID controllers for the antenna tracking system. The objective of this tuning process is to enhance tracking performance by minimizing the predefined cost function. The azimuth subsystem is

characterized by $J_{AZ} = 5$, $B_{AZ} = 0.8$, $K_t = 0.9$, $K_e = 0.9$, and $R_a = 1$, while the elevation subsystem parameters are given by $J_{EL} = 4$, $B_{EL} = 0.7$, $K_t = 0.85$, $K_e = 0.85$, and $R_a = 1$. The simulation is carried out over a time horizon of 20 seconds with a sampling interval of 0.01 seconds. The reference trajectories are designed to emulate realistic line-of-sight (LOS) tracking conditions, where the desired azimuth and elevation angles are defined as $\theta_{AZ}^{ref} = 30\sin(0.2t)$ and $\theta_{EL}^{ref} = 20\cos(0.15t)$, respectively. For the GWO algorithm, a population of 20 search agents (wolves) and a maximum of 40 iterations are considered. The optimization problem is defined in a six-dimensional search space corresponding to the PID gains of both axes, with lower and upper bounds set to [0, 0, 0, 0, 0, 0] and [50, 10, 10, 50, 10, 10], respectively. This configuration ensures a fair and consistent comparison between the different optimization strategies. The initial conditions are defined as $int_{AZ}(0) = 0$, $int_{EL}(0) = 0$, $prev_{AZ}(0) = 0$, and $prev_{EL}(0) = 0$, ensuring zero initial integral action and zero previous tracking error for both axes. The obtained gain on each technique is represented in the Tables 5.1, 5.2, 5.3, 5.4.

Table 5.1: PSO-PID and GWO-PID Gains

Axis	**Kp**	**Ki**	**Kd**
AZ	50	10	10
EL	50	10	10

Table 5.2: ACO-PID Optimal Gains

Axis	**Kp**	**Ki**	**Kd**
AZ	185.2157	38.2170	25.4781
EL	192.7392	31.3734	29.2483

Table 5.3: ACO-SMC-PID Gains

Axis	**Kp**	**Ki**	**Kd**	λ	K_{smc}
AZ	43.6210	11.6344	3.7804	5.2852	6.8091
EL	36.0983	18.2711	5.3310	13.4657	8.7651

Table 5.4: Ziegler–Nichols PID Gains

Axis	**Kp**	**Ki**	**Kd**
AZ	28.0	6.5	1.2
EL	24.5	5.8	1.0

The control effort responses presented in Fig. 5.1 highlight clear differences between the considered control strategies. The ACO-PID controller exhibits a smooth transient with

a very low torque amplitude and rapid convergence to zero, indicating an efficient and well-optimized control action. Similarly, the GWO-PID controller achieves fast stabilization, although with a slightly higher initial peak, reflecting a more aggressive response. In contrast, the PID-SMC approach shows noticeably high-frequency oscillations (chattering), which may degrade actuator lifespan despite its robustness. The PSO-SMC controller improves upon this behavior by reducing chattering, yet small residual oscillations remain. On the other hand, the classical ZN tuned PID controller produces a significantly large initial control effort with pronounced overshoot, revealing poor energy efficiency and potential actuator saturation issues. Overall, the metaheuristic-based PID controllers, particularly ACO-PID, provide the best compromise between fast transient response, smooth control action, and reduced energy consumption.

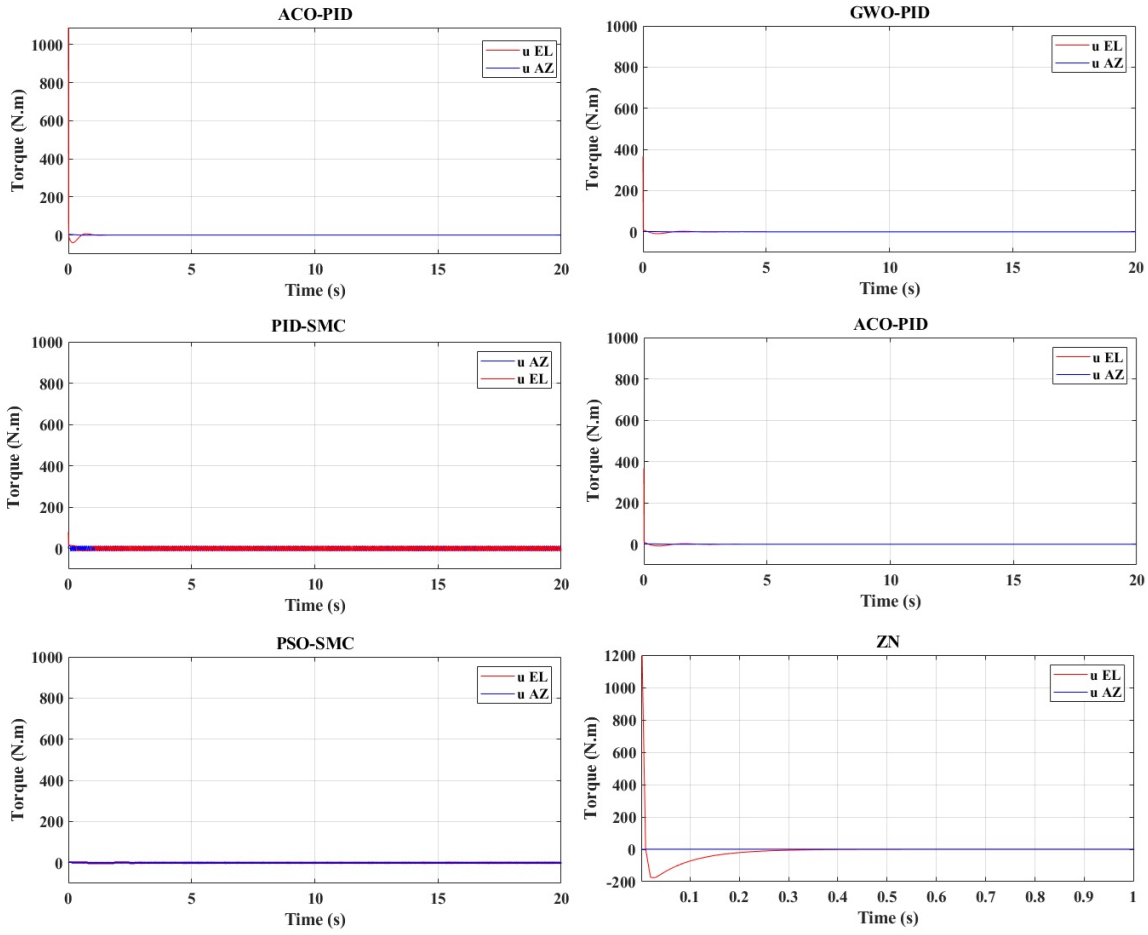


Figure 5.1: Control signals under different approaches

The tracking error responses for the different control strategies are illustrated in Fig. 5.2. It is evident that all intelligent optimization-based PID controllers (ACO-PID, GWO-PID, and PSO-PID) significantly improve the transient performance compared to the classical Ziegler–Nichols (ZN) tuning method. Specifically, these approaches exhibit faster convergence, reduced oscillations, and lower steady-state error. Among them, the SMC-based hybrid controllers demonstrate superior performance, where the SMC-GWO approach achieves a rapid error reduction with minimal oscillatory behavior, while the proposed SMCPID-ACO method

provides the best overall performance with near-zero steady-state error and very fast settling time. In contrast, the ZN method shows larger overshoot, longer settling time, and persistent oscillations. These results confirm that integrating optimization techniques with sliding mode control enhances robustness and tracking accuracy, making the proposed SMCPID-ACO controller the most effective among the evaluated strategies.

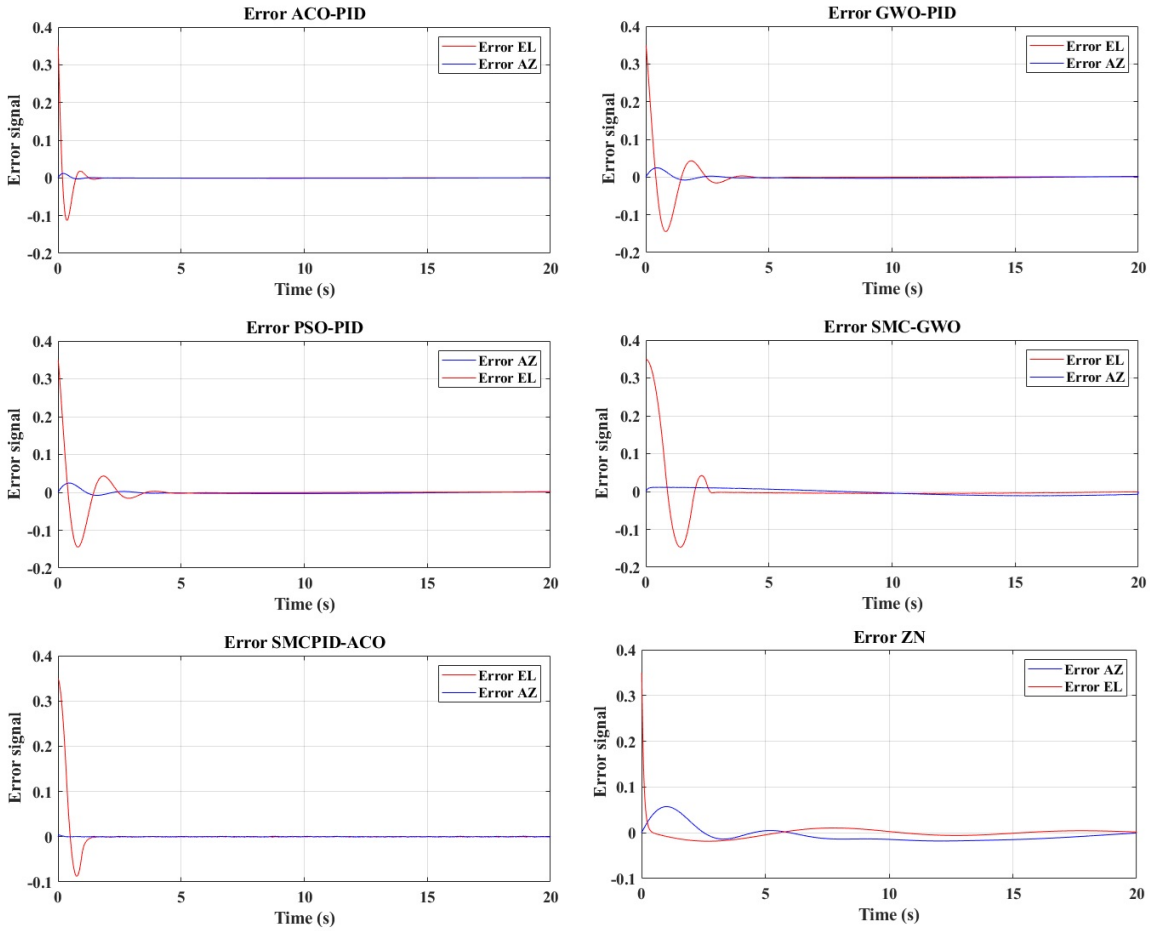


Figure 5.2: Error signals under different approaches

The angular velocity responses corresponding to the evaluated control strategies are presented in Fig. 5.3. It can be observed that the optimization-based PID controllers (ACO-PID, GWO-PID, and PSO-PID) improve the transient behavior compared to the classical Ziegler–Nichols (ZN) method, exhibiting reduced oscillations and faster damping. However, noticeable overshoot and oscillatory dynamics are still present, particularly in the GWO-PID and PSO-PID cases. In contrast, the hybrid approaches that incorporate sliding mode control demonstrate enhanced dynamic performance. The GWO-SMC controller achieves smoother convergence with reduced oscillations, although some transient peaks remain. The GWO-SMCPID method further improves stability but introduces slight high-frequency fluctuations due to the switching nature of the sliding mode component. Notably, the proposed hybrid configurations provide a better trade-off between convergence speed and robustness. Meanwhile, the ZN-tuned controller exhibits significant overshoot and slower settling, confirming its limited effectiveness for precise velocity tracking. Overall, the results highlight that combining

optimization techniques with sliding mode control leads to improved damping characteristics and more accurate angular velocity responses.

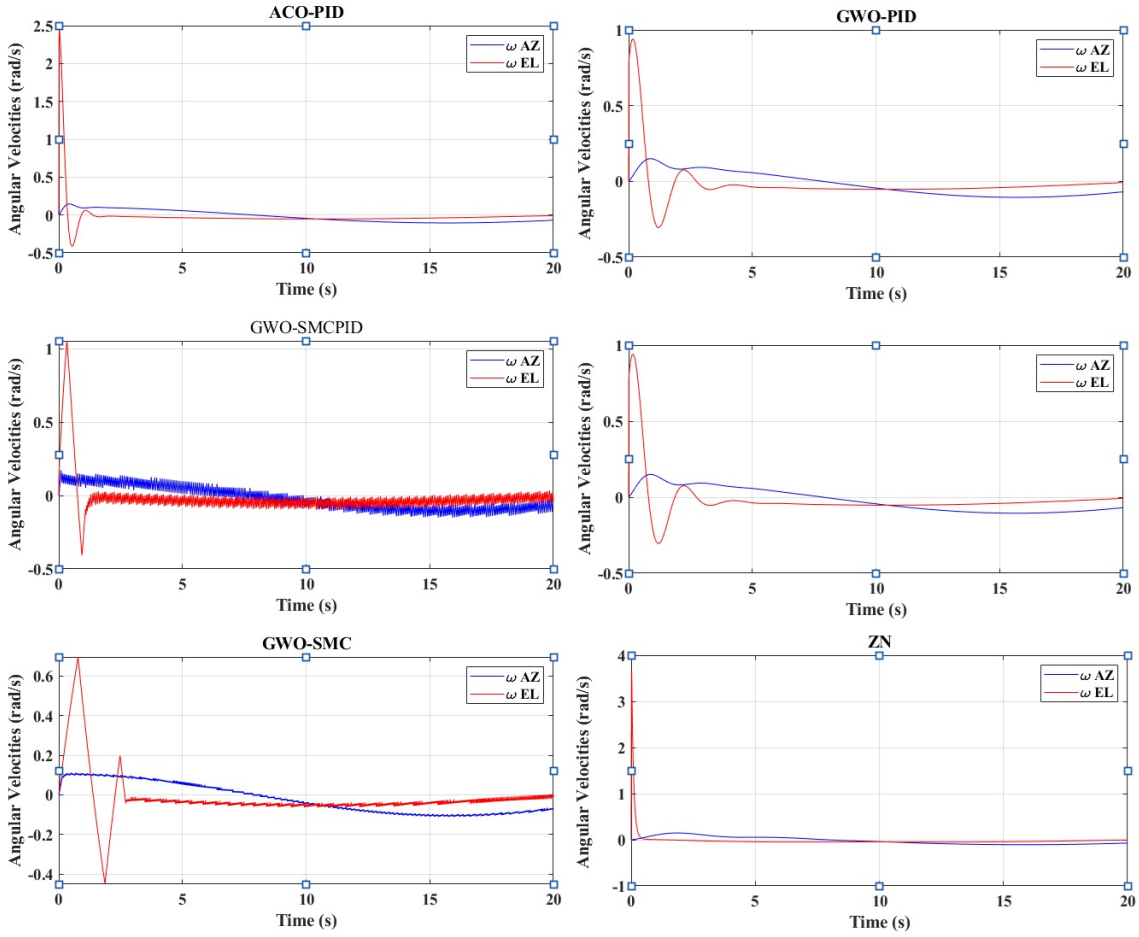


Figure 5.3: Velocities signals under different approaches

The position tracking performance of the different control strategies is depicted in Fig. 5.4. It is clear that all optimization-based PID controllers (ACO-PID, GWO-PID, and PSO-PID) achieve satisfactory tracking of the reference trajectories, with relatively small steady-state error and acceptable transient behavior. However, slight overshoot and initial oscillations are observed, particularly in the PSO-PID and GWO-PID responses. The integration of sliding mode control further enhances the tracking accuracy and robustness. In particular, the GWO-SMC and GWO-SMCPID controllers exhibit excellent agreement with the reference signals, characterized by fast convergence, minimal overshoot, and negligible steady-state error. The proposed GWO-SMCPID approach provides the most precise tracking performance, closely following the desired trajectories for both elevation and azimuth angles. In contrast, the classical Ziegler–Nichols (ZN) tuning method shows comparatively larger deviation from the reference, especially during the transient phase, along with slower convergence. These results demonstrate that hybrid controllers combining optimization algorithms with sliding mode control significantly improve trajectory tracking performance and system robustness.

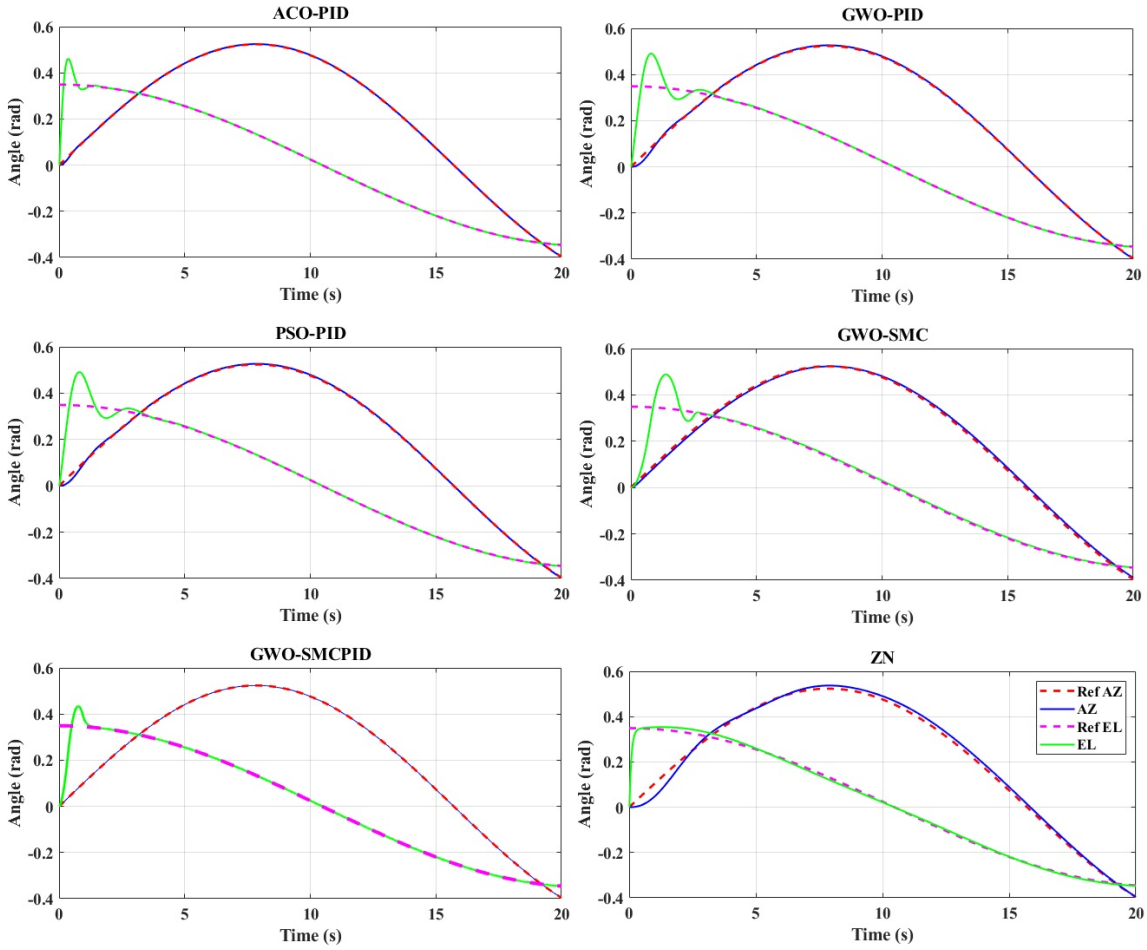


Figure 5.4: Positions signals under different approaches

The performance of the proposed control strategies is evaluated using the Integral of Time-weighted Absolute Error (ITAE) [47], which is adopted as the primary objective function to quantify tracking accuracy while penalizing long-lasting errors. A comprehensive comparison is carried out between different control configurations, including PSO-PID, GWO-PID, ACO-PID, and SMC, and the proposed hybrid ACO-SMC-PID scheme. The obtained results clearly demonstrate that the choice of optimization algorithm and control structure has a significant impact on system performance. According to the Table 5.5, the PSO-PID and GWO-PID controllers yield similar performance, with total ITAE values of 0.642777, indicating acceptable tracking but relatively moderate accuracy compared to more advanced approaches. In contrast, the ACO-PID controller significantly improves performance, achieving a reduced total ITAE of 0.149261, which highlights the effectiveness of Ant Colony Optimization in tuning PID gains for the antenna tracking system. The standalone SMC approach without optimization exhibits the highest ITAE value (2.576095), reflecting strong robustness limitations when used without proper tuning. However, when SMC is combined with PID (ACO-SMC-PID), a substantial improvement is achieved, reducing the total ITAE to 0.179931. This hybrid strategy benefits from the smooth tracking behavior of the PID controller and the robustness of the sliding mode term, leading to improved transient performance and reduced steady-state error. Finally, the results confirm that hybrid nonlinear

control strategies provide superior performance compared to classical linear controllers optimized by metaheuristic algorithms.

Table 5.5: ITAE Performance Comparison

Controller	**ITAE AZ**	**ITAE EL**	**ITAE Total**
PSO-PID	0.353204	0.289573	0.642777
GWO-PID	0.353204	0.289573	0.642777
ACO-PID	0.089876	0.059385	0.149261
SMC (no tuning)	1.612188	0.963907	2.576095
ACO-SMC-PID	0.073198	0.106733	**0.179931**

5.3 Conclusion

This chapter presented a comprehensive performance evaluation of several control strategies for antenna tracking, including classical PID tuning, metaheuristic-optimized PID controllers, and hybrid nonlinear approaches. The comparison, based on the ITAE criterion and supported by time-domain responses, clearly demonstrates that the controller structure and tuning methodology play a crucial role in achieving high tracking performance. The results show that metaheuristic algorithms significantly enhance PID performance compared to the classical ZN method, with ACO-PID providing the best results among the standalone PID controllers due to its superior optimization capability. However, the standalone SMC approach, despite its robustness, suffers from poor performance when not properly tuned, as reflected by its high ITAE value and oscillatory behavior.

The most important outcome of this study is the effectiveness of hybrid control strategies. By combining the robustness of sliding mode control with the smoothness and adaptability of PID regulation, the proposed ACO-SMC-PID controller achieves a substantial improvement in tracking accuracy, transient response, and robustness. This is evidenced by reduced tracking errors, faster convergence, improved damping characteristics, and more efficient control effort compared to other methods. Although slight chattering effects remain in SMC-based approaches, the integration with optimized PID significantly mitigates these issues, resulting in a well-balanced control performance. Overall, the findings confirm that hybrid nonlinear controllers optimized using metaheuristic algorithms represent a powerful and reliable solution for high-precision antenna tracking systems.

Chapter 6

General Conclusions

This thesis has presented the design, optimization, and performance evaluation of advanced control strategies for a two-axis (azimuth–elevation) antenna tracking system. The primary objective was to improve tracking accuracy, robustness, and dynamic performance under realistic operating conditions. To achieve this goal, both classical and modern control approaches were investigated, including conventional PID controllers, Sliding Mode Control (SMC), and hybrid SMC-PID structures. In addition, several metaheuristic optimization techniques, namely Particle Swarm Optimization (PSO), Grey Wolf Optimization (GWO), and Ant Colony Optimization (ACO), were employed to optimally tune controller parameters. The simulation framework was carefully designed to ensure realistic behavior and fair comparison between all control strategies. The antenna system parameters for both axes were selected to represent a practical electromechanical model. The azimuth subsystem is characterized by $J_{AZ} = 5$, $B_{AZ} = 0.8$, $K_t = 0.9$, $K_e = 0.9$, and $R_a = 1$, while the elevation subsystem is defined by $J_{EL} = 4$, $B_{EL} = 0.7$, $K_t = 0.85$, $K_e = 0.85$, and $R_a = 1$. The system is simulated over 20 seconds with a sampling time of 0.01 seconds. The reference trajectories are defined as $\theta_{AZ}^{ref} = 30\sin(0.2t)$ and $\theta_{EL}^{ref} = 20\cos(0.15t)$, representing realistic line-of-sight tracking conditions.

In order to ensure a stable and unbiased initialization of the control system, all internal states were set to zero at the beginning of the simulation. In particular, the integral actions were initialized as $int_{AZ}(0) = 0$ and $int_{EL}(0) = 0$, while the previous error values were set as $prev_{AZ}(0) = 0$ and $prev_{EL}(0) = 0$. This guarantees that no artificial transients or residual control actions affect the initial system response. The obtained results clearly show that classical tuning methods such as Ziegler–Nichols are not suitable for high-precision antenna tracking applications. Although simple to implement, this method leads to significant overshoot, long settling time, and persistent oscillations, which degrade overall system performance. In contrast, optimization-based PID controllers significantly improve system behavior. Among them, ACO-PID demonstrates superior performance compared to PSO-PID and GWO-PID, achieving better tuning quality and reduced tracking error. However, while these methods enhance performance, they still exhibit limitations in terms of robustness and transient oscillations.

A more advanced improvement is achieved through Sliding Mode Control (SMC), which

provides strong robustness against disturbances and model uncertainties. Nevertheless, standalone SMC suffers from chattering phenomena and sensitivity to parameter tuning, which may affect smooth operation. In order to overcome these limitations, hybrid control strategies combining SMC with PID control are introduced. The integration of both methods allows the system to benefit from the robustness of sliding mode control and the smooth response of PID regulation. In particular, optimization-enhanced hybrid structures significantly improve performance. The SMC-GWO approach achieves rapid error reduction with minimal oscillatory behavior, demonstrating strong dynamic response and improved stability. More importantly, the proposed SMCPID-ACO method provides the best overall performance among all tested controllers. It achieves near-zero steady-state error, very fast settling time, and highly stable convergence behavior. In contrast, the classical Ziegler–Nichols method remains the weakest, showing large overshoot and slow response.

The angular velocity and position tracking analyses further confirm these findings. Optimization based controllers improve transient response compared to classical methods, but hybrid SMC-based controllers clearly outperform them by providing smoother dynamics, faster convergence, and higher tracking precision. Among all tested approaches, hybrid controllers consistently achieve the best balance between speed, accuracy, and robustness. Quantitative evaluation using the Integral of Time-weighted Absolute Error (ITAE) confirms these observations. Optimization-based PID controllers reduce tracking error significantly compared to classical tuning. The standalone SMC shows the highest error due to a lack of tuning optimization. However, the hybrid ACO-SMC-PID controller achieves the lowest ITAE value, demonstrating its superiority in minimizing both transient and steady-state errors.

In conclusion, this work demonstrates that combining nonlinear control techniques with metaheuristic optimization forms a powerful and effective framework for antenna tracking systems. Hybrid optimized controllers significantly enhance robustness, accuracy, and dynamic performance compared to classical approaches. Among all evaluated strategies, the proposed optimized hybrid SMC-PID structure represents the most effective solution for high-precision tracking applications. Future work may focus on experimental validation, real-time implementation, and the integration of intelligent adaptive techniques such as neural networks or reinforcement learning to further improve performance under uncertainty and external disturbances.

References

[1] S. Karmous, N. Adem, M. Atiquzzaman, and S. Samarakoon, "How can optical communications shape the future of deep space communications? a survey," *IEEE Communications Surveys & Tutorials*, vol. 27, no. 1, pp. 725–747, 2024.

[2] Z. Sun, *Technologies for deep space exploration*. Springer, 2021.

[3] D. S. Abraham, Y. Chen, D. P. Heckman, L. Heid, A. Kwok, B. E. MacNeal, K. Tran, and H. Xie, "Future deep space mission communications trends and their implications for nasa's deep space network," in *International conference on space operations*. Springer, 2023, pp. 373–419.

[4] W. A. Imbriale, *Large antennas of the deep space network*. John Wiley & Sons, 2005.

[5] W. Gawronski, "Control and pointing challenges of large antennas and telescopes," *IEEE Transactions on Control Systems Technology*, vol. 15, no. 2, pp. 276–289, 2007.

[6] A. M. d. Almeida, M. K. Lenzi, and E. K. Lenzi, "A survey of fractional order calculus applications of multiple-input, multiple-output (mimo) process control," *Fractal and Fractional*, vol. 4, no. 2, p. 22, 2020.

[7] C. C. Hang, K. J. Åström, and W. K. Ho, "Refinements of the ziegler–nichols tuning formula," in *IEE Proceedings D (Control Theory and Applications)*, vol. 138, no. 2. IET, 1991, pp. 111–118.

[8] M. Y. Silaa, M. Derbeli, O. Barambones, C. Napole, A. Cheknane, and J. M. Gonzalez de Durana, "An efficient and robust current control for polymer electrolyte membrane fuel cell power system," *Sustainability*, vol. 13, no. 4, p. 2360, 2021.

[9] M. Roslan, A. Q. Al-Shetwi, M. Hannan, P. Ker, and A. Zuhdi, "Particle swarm optimization algorithm-based pi inverter controller for a grid-connected pv system," *PloS one*, vol. 15, no. 12, p. e0243581, 2020.

[10] J. H. Holland, "Genetic algorithms," *Scientific american*, vol. 267, no. 1, pp. 66–73, 1992.

[11] M. Y. Silaa, O. Barambones, M. Derbeli, C. Napole, and A. Bencherif, "Fractional order pid design for a proton exchange membrane fuel cell system using an extended grey wolf optimizer," *Processes*, vol. 10, no. 3, p. 450, 2022.

[12] M. Dorigo and T. Stützle, "Ant colony optimization: overview and recent advances," *Handbook of metaheuristics*, pp. 311–351, 2018.

[13] K. V. Price, "Differential evolution," in *Handbook of optimization: From classical to modern approach*. Springer, 2013, pp. 187–214.

[14] Z. Hasan, K. Salman, and M. E. El-Hawary, "Linear quadratic regulator design for power system stabilizer using biogeography based optimization method," in *2016 IEEE Canadian Conference on Electrical and Computer Engineering (CCECE)*. IEEE, 2016, pp. 1–6.

[15] R. Guardeño, M. J. López, and V. M. Sánchez, "Mimo pid controller tuning method for quadrotor based on lqr/lqg theory," *Robotics*, vol. 8, no. 2, p. 36, 2019.

[16] M. Y. Silaa, I. Rougab, A. Bencherif, O. Barambones, and N. Benaya, "Integral terminal sliding mode control for 2-dof robot manipulators enhanced by evolutionary algorithm under external disturbances," 2025.

[17] M. Y. Silaa, M. Derbeli, O. Barambones, and A. Cheknane, "Design and implementation of high order sliding mode control for pemfc power system," *Energies*, vol. 13, no. 17, p. 4317, 2020.

[18] M. Y. Silaa, I. Rougab, O. Barambones, and A. Bencherif, "Hybrid fuzzy-smc controller with pso for autonomous underwater vehicle," in *Actuators*, vol. 15, no. 2. MDPI, 2026, p. 90.

[19] M. Y. Silaa, A. Bencherif, and O. Barambones, "A novel robust adaptive sliding mode control using stochastic gradient descent for pemfc power system," *International Journal of Hydrogen Energy*, vol. 48, no. 45, pp. 17 277–17 292, 2023.

[20] L. A. T. Aly, "Emotion-driven physiological actor dynamics for interactive theatre sound," Ph.D. dissertation, Universidade do Porto (Portugal), 2024.

[21] W. Rafferty, S. D. Slobin, C. T. Stelzried, and M. K. Sue, "Ground antennas in nasa's deep space telecommunications," *Proceedings of the IEEE*, vol. 82, no. 5, pp. 636–645, 2002.

[22] A. A. Mulla and P. N. Vasambekar, "Overview on the development and applications of antenna control systems," *Annual Reviews in Control*, vol. 41, pp. 47–57, 2016.

[23] J. Armstrong, F. Estabrook, S. Asmar, L. Iess, and P. Tortora, "Reducing antenna mechanical noise in precision spacecraft tracking," *Radio Science*, vol. 43, no. 03, pp. 1–7, 2008.

[24] Q. Xu, F. Xue, H. Wang, and L. Yi, "Measurement and correction of pointing error caused by radio telescope alidade deformation based on biaxial inclination sensor," *Micromachines*, vol. 14, no. 7, p. 1283, 2023.

[25] A. Al-Mayyahi, A. Aldair, Z. A. Khalaf, and W. Wang, "Control system design for azimuth position of earth station antennas," *Journal of Engineering and Applied Science*, vol. 71, no. 1, p. 199, 2024.

[26] D. Motors and D. Daw-son, "Control systems technology."

[27] M. B. Aremu, M. Abdel-Nasser, N. M. Alyazidi, and S. El-Ferik, "Disturbance observer-based bio-inspired lqr optimization for dc motor speed control," *IEEE Access*, vol. 12, pp. 152 418–152 429, 2024.

[28] Z. Marinković, D. Marinković, G. Petrović, and P. Milić, "Modelling and simulation of dynamic behaviour of electric motor driven mechanisms," *Tehnicki vjesnik/Technical Gazette*, vol. 19, no. 4, pp. 717–725, 2012.

[29] S. A. Shaikh and I. Tekin, "Two axis direction finding antenna system using sum–difference patterns in x band," *Microwave and Optical Technology Letters*, vol. 57, no. 9, pp. 2085–2092, 2015.

[30] B. K. Bose, "Power electronics and motor drives recent progress and perspective," *IEEE transactions on industrial electronics*, vol. 56, no. 2, pp. 581–588, 2008.

[31] S. Li, J. Tang, B. Zheng, L. Zhu, C. Yang, N. Zhao, X. Y. Zhang, and K.-K. Wong, "Rotatable antenna system empowered low-altitude economy: Opportunities and challenges," *IEEE Wireless Communications*, 2025.

[32] S. J. Ovaska and S. Valiviita, "Angular acceleration measurement: A review," in *IMTC/98 Conference Proceedings. IEEE Instrumentation and Measurement Technology Conference. Where Instrumentation is Going (Cat. No. 98CH36222)*, vol. 2. IEEE, 1998, pp. 875–880.

[33] T. Golani and S. Sabhapathy, "Analytic model of wind disturbance torque on servo tracking antenna," *Int. J. Mod. Eng. Res*, vol. 3, no. 5, pp. 3242–3247, 2013.

[34] J. Margielewicz, D. Gąska, and G. Litak, "Modelling of the gear backlash," *Nonlinear Dynamics*, vol. 97, no. 1, pp. 355–368, 2019.

[35] C. Gonzáles Diaz and P. Gardonio, "Proportional, integral, derivative, pid-, pi-and pd-velocity feedback control with inertial actuators," 2005.

[36] Electronics Coach. (n.d.) Proportional integral (pi) controller. [Online]. Available: https://electronicscoach.com/proportional-integral-controller.html

[37] X. Zhang, H. Li, and M. Shao, "Fixed-time-convergent sliding mode control with sliding mode observer for pmsm speed regulation," *Sensors*, vol. 24, no. 5, p. 1561, 2024.

[38] M. Y. Silaa, O. Barambones, A. Bencherif, and I. Rougab, "An adaptive control strategy with switching gain and forgetting factor for a robotic arm manipulator," *Machines*, vol. 13, no. 5, p. 424, 2025.

[39] I. M. Boiko, "Chattering in sliding mode control systems with boundary layer approximation of discontinuous control," *International Journal of Systems Science*, vol. 44, no. 6, pp. 1126–1133, 2013.

[40] V. I. Utkin, *Sliding modes in control and optimization*. Springer Science & Business Media, 2013.

[41] V. V. Patel, "Ziegler-nichols tuning method: Understanding the pid controller," *Resonance*, vol. 25, no. 10, pp. 1385–1397, 2020.

[42] T. J. McAvoy, "Time optimal and ziegler-nichols control. experimental and theoretical results," *Industrial & Engineering Chemistry Process Design and Development*, vol. 11, no. 1, pp. 71–78, 1972.

[43] F. Marini and B. Walczak, "Particle swarm optimization (pso). a tutorial," *Chemometrics and intelligent laboratory systems*, vol. 149, pp. 153–165, 2015.

[44] S. Mirjalili, S. M. Mirjalili, and A. Lewis, "Grey wolf optimizer," *Advances in engineering software*, vol. 69, pp. 46–61, 2014.

[45] M. Dorigo, "Ant colony optimization," *Scholarpedia*, vol. 2, no. 3, p. 1461, 2007.

[46] S. Mishra, S. Roy, A. Routray, S. C. Swain, and P. K. Sadhu, "Enhanced fault classification in underground cable systems: a three-step framework utilizing evolutionary optimization for signal tracking and parameter estimation," *Microsystem Technologies*, vol. 30, no. 10, pp. 1325–1340, 2024.

[47] M. Y. Silaa, O. Barambones, J. A. Cortajarena, P. Alkorta, and A. Bencherif, "Pemfc current control using a novel compound controller enhanced by the black widow algorithm: A comprehensive simulation study," *Sustainability*, vol. 15, no. 18, p. 13823, 2023.